Heterogeneity Modeling and Geopseudo Upscaling Applied to Waterflood Performance Prediction of an Incised Valley Reservoir: Countess YY Pool, Southern Alberta, Canada[1]

Madeleine Peijs-van Hilten,[2] Timothy R. Good,[3] and Brian A. Zaitlin[4]

ABSTRACT

The objective of this study is to analyze the effects of different modeling approaches and various scales of geological heterogeneity on waterflood recovery and volumetrics of an incised valley reservoir. Seismic, well-log, and core data are integrated with an incised valley facies model to create cross sections used to perform two-phase 2-D (two-dimensional) fluid-flow simulations.

Core observations and probe-permeameter data are acquired to perform a geopseudo upscaling exercise, which simulates the effects of small-scale sedimentary structures on fluid flow. Applying this method and incorporating small-scale sedimentary structures in 2-D fluid flow simulations have proved to make a significant difference in individual-well oil recovery (up to 8%) depending on the facies types involved in a well's drainage area. Incorporating variations in sand-body dimensions and connectivities has proved to have a major impact on field oil recovery (30% difference between extreme 2-D cases), whereas variations in incised valley size have the greatest impact on original oil-in-place values (21% between extreme 2-D cases).

A layercake model of an incised valley reservoir results in optimistic performance compared to a geopseudo upscaled model (11% higher oil recovery for a 2-D case). In a highly favorable scenario, an incised valley reservoir indeed may behave like a layercake, but it is more likely that it will not perform as well.

Not taking into account small-scale sedimentary structures, uncertainty in reservoir architecture, and incised valley size in reservoir simulation studies can introduce substantial errors in reserves estimation and production forecasting. Lessons learned from this 2-D study will be used in a future full-field three-dimensional waterflood simulation of the Countess YY pool.

[1]Manuscript received April 2, 1997; revised manuscript received February 24, 1998; final acceptance March 21, 1998.

[2]Graduate of Heriot-Watt University. Current address: Halliburton Energy Services, Reservoir Description, 91-1SE–25J, 10200 Bellaire Boulevard, Houston, Texas 77072-5299; e-mail: madeleine.peijs@halliburton.com

[3]Mobil Technology Company, 13777 Midway Road, Dallas, Texas 75244-4390; e-mail: tim_good@email.mobil.com

[4]PanCanadian Petroleum Limited, 150 9th Avenue S.W., P.O. Box 2850, Calgary, Alberta, Canada T2P 2S5; e-mail: zaitlin@earthlink.net

This research project was done as the final part of a Master's degree program in reservoir evaluation and management at the Petroleum Engineering Department of Heriot-Watt University in Edinburgh, Scotland. Many individuals provided assistance so that this study could be completed within the available period of three months. The Petroleum Engineering Department is acknowledged for providing computer facilities and probe-permeameter equipment. Philip Ringrose and Gillian Pickup are thanked for helpful information and discussions on geopseudo upscaling. We gratefully acknowledge PanCanadian Petroleum Limited, who operates the Countess YY Pool, for organizing and financing this project, for access to the data and the core facility, and for permission to publish this work. We especially thank Eugene Peters and Garth Syhlonyk for sharing their knowledge on the Countess YY pool and incised valley reservoirs in general. Reviews of the manuscript by Bob Dalrymple, Eugene Peters, Janok Bhattacharya, I. M. Yarus, and an anonymous reviewer are very much appreciated.

INTRODUCTION

Some of the largest hydrocarbon reservoirs in the world are hosted by fluvial and estuarine sandstones deposited within incised valley systems. Examples are the Cusiana field in Colombia (Pulham, 1994), the Messla-Faregh field in Libya (Halbouty, 1982), and the Cut Bank field in Montana in the United States (Dolson et al., 1993). These reservoirs exhibit highly complex stratigraphic relationships as a result of relative sea level fluctuations and shifting depositional systems. Understanding the geometry, spatial distribution, and reservoir characteristics of facies in an incised valley system is potentially of major importance to hydrocarbon production optimization.

Reservoirs are commonly analyzed with the help of reservoir simulation and visualization software. The level of reservoir description detail used in a simulation model depends on field size, reservoir

AAPG Bulletin, V. 82, No. 12 (December 1998), P. 2220–2245.

heterogeneity, computer capacity, and available resources (time, people, budget). Reservoir engineers commonly ask geologists to provide them with a simplified geological model; for example, a layercake representation of the reservoir. Even if a detailed geological model does exist, it usually will be averaged in an upscaling process so that the reservoir simulator can perform faster; however, the consequence is that simulation results may not be accurate or may deviate from reality. This issue is addressed in the work described here using data from the Countess YY pool, an incised valley reservoir, under waterflood, located in southern Alberta, Canada (Figure 1).

OBJECTIVES

The first objective of this study is to quantitatively compare simulation results of three reservoir modeling approaches with a varying degree of reservoir description detail.

(1) A simple layercake model with reservoir properties from core-plug data averaged per layer.

(2) A reservoir architecture model with a facies distribution based on field data and the incised valley facies model as proposed by Dalrymple et al. (1992) and Zaitlin et al. (1994). Reservoir properties from core-plug data are averaged per facies. This model is more realistic than the layercake model in terms of geometry, spatial distribution, and properties of the reservoir units.

(3) A similar reservoir architecture model simulated using results from a geopseudo upscaling exercise. The geopseudo upscaling technique incorporates successive scales of geological heterogeneity into effective flow functions, starting with small-scale sedimentary structures such as crossbedding. The probe-permeameter is applied to characterize these structures. This model not only has a more realistic reservoir architecture, but it also includes a more realistic characterization of the fluid-flow behavior of the various facies.

We suggest that the geopseudo upscaled model comes closest to reality, but this cannot be verified with two-dimensional (2-D) models. This study is a first step toward a full-field three-dimensional (3-D) simulation study that will be done to optimize production of the Countess YY pool. Only then is a direct comparison between simulation results and actual production data possible. Results presented here serve the purpose only of improving understanding.

The second objective is to quantitatively assess the impact of several scales of geological heterogeneity on waterflood recovery and volumetrics by simulating and comparing the results of a range of 2-D sensitivity models.

(1) Microscale heterogeneity represented by small-scale sedimentary structures is accounted for by using the geopseudo upscaling approach. The impact of this approach can be assessed by comparing its results to those of a conventionally averaged or upscaled model.

(2) Mesoscale heterogeneity is represented by the incised valley reservoir architecture or internal facies distribution, which is constrained by well data. The uncertainty in the interwell region allows modeling of a number of possible realizations of the facies distribution and involves varying sand-body or reservoir-unit dimensions and connectivities.

(3) Macroscale heterogeneity is represented by the incised valley container size and shape, and is constrained by well and seismic data. The uncertainty caused by seismic resolution limitations and interpretation pitfalls allows modeling of a number of possible realizations of the container size.

INCISED VALLEY SYSTEM

Conceptual Model

A conceptual incised valley facies model was proposed by Dalrymple et al. (1992) and Zaitlin et al. (1994). They defined criteria to recognize an incised valley system and its basal sequence boundary from subsurface data. The valley is initiated by incision and fluvial erosion during a fall in relative sea level; once sea level starts to rise again, initial deposition is by fluvial systems. During transgression, a variety of fluvial, estuarine, and marine environments migrate up the valley. The depositional succession can be divided vertically into a set of systems tracts separated by erosional and flooding surfaces. Individual sequences may show progradation, but repeated backstepping of the sequences occurs due to the ongoing transgression. The succession can be divided longitudinally into three segments, each with a unique facies association. The stratigraphic organization of the various facies can be complex in these systems. The framework provided in this model is an aid in delineating and predicting reservoir facies.

Countess YY Pool

The Countess YY pool is one of several incised valley reservoirs located beneath Lake Newell in southern Alberta, Canada. These pools are within the regional Countess-Alderson trend, which is part of the much larger Glauconitic channel system that extends in excess of 515 km from the lowstand shoreline deposits at the Hoadley barrier-bar

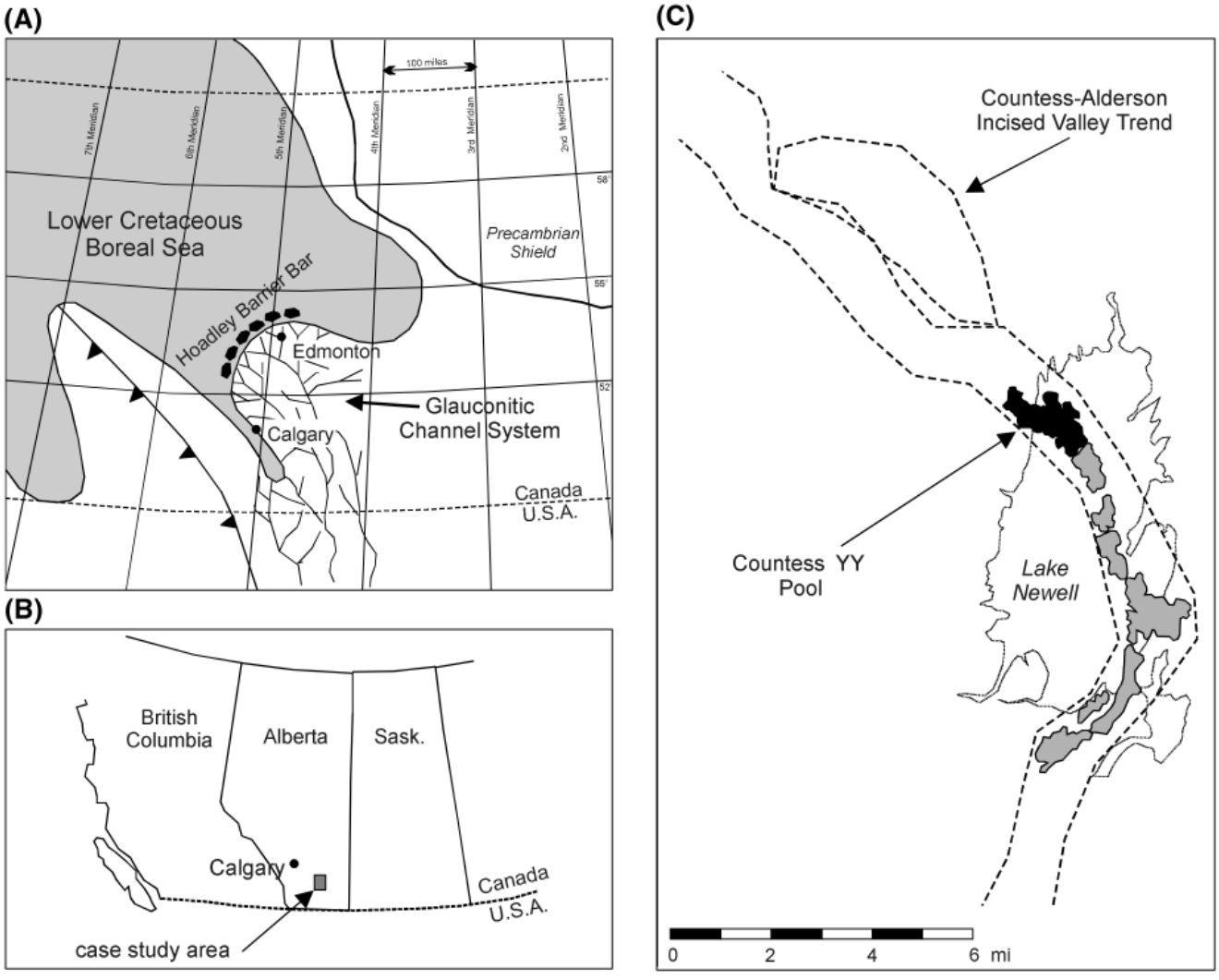

Figure 1—(A) Lower Cretaceous paleogeography showing the extent of the Glauconitic channel system. (B) Map showing the location of the case study area in southern Alberta, Canada. (C) Case study area map showing the regional Countess-Alderson incised valley trend (dashed outline) and the location of the Countess YY pool beneath Lake Newell (modified after Broger et al., 1997).

system southward to northern Montana (Figure 1A). This channel system has an inferred northward-trending paleodrainage toward the Lower Cretaceous Boreal Sea. The Lake Newell area of the Countess-Anderson trend is interpreted to lie within segment 1 of a wave-dominated incised valley system (Broger et al., 1997), generally characterized by backstepping, lowstand to transgressive fluvial and estuarine deposits overlain by transgressive marine sands or shelf muds.

Figure 2 shows the stratigraphic column that applies to this region. The producing unit is the Lower Glauconite channel that incises into the shallow-marine regional Glauconite cycles. The low-permeability Middle Glauconite channel incises into the producing channel, thus forming a compound incised valley system. Locally, the Middle Glauconite channel forms an updip seal to trap hydrocarbons in the Lower Glauconite channel.

The Lower Glauconite channel has been identified from subsurface data by Broger et al. (1997) using the criteria defined in the conceptual incised valley model. Cores show a sharp erosional contact between the stratigraphically lower Detrital member and the Lower Glauconite deposits, a contact that is identified as the basal sequence boundary of the system. The contact between regional Glauconitic shallow-marine and Lower Glauconitic fluvial or estuarine deposits is interpreted as a basinward shift in facies occurring across the sequence

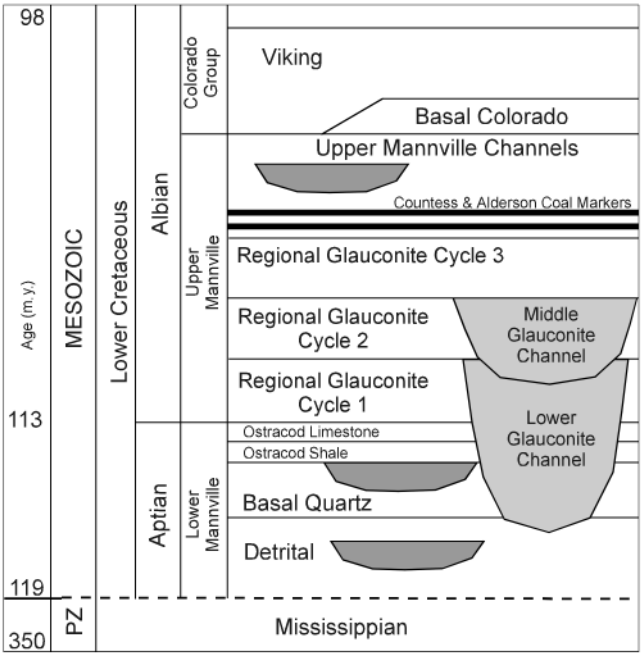

Figure 2—Informal stratigraphic column for the Lower Cretaceous in the case study area (modified after Broger et al., 1997).

boundary. Figure 3 shows a structural cross section of the Countess YY pool interpreted from seismic and well data. The incised valley system truncates regional formations, and the sequence boundary is mappable from the base of the system onto the interfluve area.

FACIES DESCRIPTIONS

In their paper, Broger et al. (1997) gave detailed lithological descriptions of the various facies they recognized in both Glauconite channels. For the purpose of fluid-flow simulation, it is important to distinguish facies or flow units with characteristic reservoir properties, which may influence fluid-flow patterns in different ways; therefore, a reinterpretation of the facies has been done here for the Countess YY pool using core data from 4 wells and log curve data from 17 wells. Core-plug-averaged reservoir properties for each of the facies described below are given in Table 1.

Applying the geopseudo upscaling approach in fluid-flow simulation requires acquisition of detailed data on the sedimentary structures present in each facies. Measurements on the thickness of structures, such as cross-bedding laminae, mud drapes, interval thicknesses, and angles of cross-bedding and inclination, were taken from the cored wells. The averaged values are given in Table 2. Note that for some measurements a bimodal distribution was found, resulting in two averaged values.

In addition to core observations, pressure decay probe-permeameter data have been acquired. A number of halved cores were sampled every 2 mm using a small probe tip with an internal diameter of 1.22 mm, a size found suitable to capture the permeability contrast even across thin mud drapes. Representative values for each structure have been selected and statistically analyzed (Table 3).

Lower Glauconite channel

Fluvial Facies

These sediments consist of litharenitic, coarse- to medium-grained, large-scale trough and planar-tabular cross-bedded sandstone successions with basal erosional surfaces that are usually overlain by a pebble lag. This facies has excellent reservoir quality and commonly is encountered at the base of the incised valley system; facies thickness ranges from 1 to more than 10 m. The gamma-ray log signature shows a blocky or sometimes fining-upward profile with a high peak at the base. The sediments are interpreted to be deposited by a highly connected and continuous-braided to coarse-grained meandering fluvial channel system.

The most common structure present is tabular/planar foreset cross-bedding interpreted to originate from dune migration processes. Cross-bedding is expressed by segregation of chert (gray, dark) and quartz (beige, light) particles. The average cross-bed angle is 19°, but there is large variation in the angle measurements (9–35°). This angle varies depending on the orientation of the cross-bed sets relative to the paleocurrent direction. The cores have not been oriented; therefore, the measurements represent random samples of the angle, prohibiting the generation of direction-dependent geopseudo upscaling models that can be used for simulating flow either perpendicular or parallel to the paleoflow direction. (In this study only a 2-D cross section perpendicular to the inferred paleoflow is simulated.) No bottomset lamination has been identified. The permeability contrast between the dark and light laminae is within the same order of magnitude (Table 3).

Bayhead-Delta Distributary Channel: Base and Top Facies

These sediments consist of medium- to coarse-grained, planar-tabular cross-bedded, flaser-bedded, and tidally-bedded sandstones. Massive to repetitive fining-upward successions are characterized by basal scour surfaces marked by shale rip-up clasts and channel lags. From seismic amplitude maps a northwest (downvalley) bifurcation of the facies is

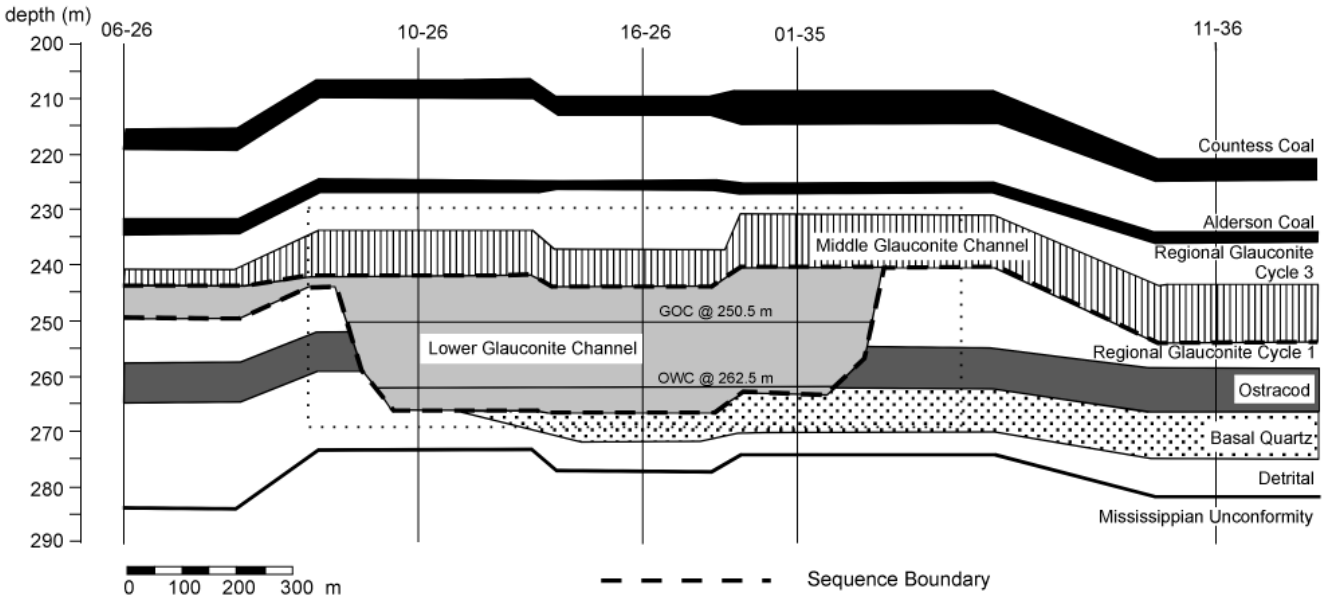

Figure 3—Structural cross section CC′ perpendicular to the incised valley trend across the center of the Countess YY reservoir (see Figure 5) showing the outline of the Lower Glauconite channel cutting into the regional geology. The dashed box refers to the part of the section represented in Figure 6C.

observed, indicating a distributary channel pattern. Evidence of tidal activity is indicated by the presence of mud drapes and couplets, as well as a typical estuarine ichnofossil assemblage. This facies has good reservoir quality and either gradationally overlies the fluvial facies or immediately overlies the basal sequence boundary. Thickness ranges from 3 to more than 11 m. The gamma-ray log signature shows an overall coarsening-upward trend, indicating a progradational environment. Individual blocky to fining-upward units of 3–7 m thickness can be identified, either as single units or stacked. This facies is interpreted to represent bayhead-delta distributary channels. Single and stacked channel units show a fining-upward and an obvious shaling-upward trend in core and on logs, with tidal mud drapes being more abundant in the upper part of the units, indicating either an increase in tidal influence or a decrease in energy during deposition. To capture this trend in the geopseudo upscaling exercise, the bayhead-delta distributary channel facies is subdivided into a base and a top part.

A variety of structures indicating tidal influences are present in this facies, but for geopseudo upscaling and fluid-flow simulation purposes, we emphasize modeling those structures that are expected to have an impact on fluid flow; i.e., the mud drapes and mud couplets. The base facies comprises structureless and

Table 1. Arithmetically Averaged Reservoir Properties per Facies Based on Core Plug or Wireline Data*

Facies Type	Porosity (Fraction)	K_h (md)	K_v (md)	K_v/K_h Ratio	Data Source
Fluvial	0.25	3118	932	0.30	Core plugs
Bayhead-delta distributary channel base	0.27	2399	1584	0.66	Core plugs
Bayhead-delta distributary channel top	0.27	2399	1584	0.66	Core plugs
IHS tidal point-bar base	0.28	3411	2388	0.70	Core plugs
IHS tidal point-bar top	0.25	1150	673	0.59	Core plugs
Delta-front turbidite sandstones	0.15–0.25	100–1000	–	–	Wireline logs
Delta-front turbidite shales	0.05	0.10	–	–	Wireline logs
Central basin	0.21	152	22	0.14	Core plugs
Marine shales	0.05	0.10	–	–	Wireline logs
Middle Glauconite channel	0.10	0.55	0.015	0.03	Core plugs

*K_v = vertical permeability, K_h = horizontal permeability.

Table 2. Averaged Values of Core Observations of Sedimentary Structures

Observation Type and Unit of Measure	Fluvial Facies	Bayhead-Delta Distributary Channel		IHS Tidal Point Bar	
		Base Facies	Top Facies	Base Facies	Top Facies
Thickness dark laminae (chert) (mm)	4	3	3	3	3
Thickness light laminae (quartz) (mm)	4	8	8	6	7
Cross-bed angle (°)	19	21	21	19	5 and 19
Thickness mud drape (mm)	No mud drapes	2	2	1	1
Spacing between mud drapes (mm)		3 and 18.5	3 and 10.5	1	2 and 7
Continuous/discontinuous mud drapes (%)		100/0	60/40	100/0	50/50
Length discontinuous mud drapes (mm)			29		25
Thickness massive interval (cm)	No massive intervals	48	No massive intervals	No massive intervals	No massive intervals
Thickness cross-bedded interval (cm)		25			
Thickness mud drape interval (cm)	No mud drapes	5	10	11	18
Spacing between mud drape intervals (cm)		200	50	32	16
Thickness inclined shale intervals (cm)	No shale intervals	No shale intervals	No shale intervals	2	2
Thickness inclined sandstone intervals (cm)				111	30
Inclination angle (°)				5 and 19	19

Table 3. Summary of Probe-Permeameter Data Analysis

Facies Type	Structure Type	Arithmetic Average (md)	Range (md)	Coefficient of Variation (md)	Number of Measurements (md)
Fluvial	Dark laminae	3263	1800–4760	0.26	29
	Light laminae	7730	5090–11,500	0.19	87
Bayhead Delta	Mud drapes	30	1–152	1.00	40
Distributary	Dark laminae	251	6–868	0.72	53
Channel Base	Light laminae	2757	487–8261	0.70	66
Bayhead Delta	Mud drapes	56	0–199	0.92	78
Distributary	Dark laminae	415	56–1054	0.73	26
Channel Top	Light laminae	2147	572–9061	0.60	119
IHS Tidal Point-	Mud drapes	61*	–	–	–
Bar Base	Dark laminae	550	101–1316	0.74	18
	Light laminae	2728	1123–5813	0.48	68
IHS Tidal Point-	Mud drapes	61	0–175	1.07	21
Bar Top	Dark laminae	550*	–	–	–
	Light laminae	2464	617–6402	0.60	34

*No structures available for measurement in core samples; value taken from the other IHS facies.

cross-bedded intervals, and intervals where the cross-bedding is accompanied by mud drapes and couplets. Bottomset lamination has been observed. The top facies does not have massive intervals, and cross-bedding occurs throughout. Compared to the base facies, intervals with mud drapes are thicker and occur more frequently, and the spacing between the mud drapes is less (Table 2). The permeability contrast between laminae in this facies is one order of magnitude, and the mud drapes and couplets are an order of magnitude lower, resulting in an overall permeability contrast of two orders of magnitude (Table 3). Figure 4 illustrates a halved core of the bayhead-delta distributary channel top facies and its corresponding probe-permeameter profile.

Inclined Heterolithics Tidal Point Bar: Base and Top Facies

These sediments are characterized by a sharp to erosive basal contact with a fining-upward trend. They form a series of inclined fining-upward cycles of fine, massive to tidally bedded, flaser-bedded sandstones, alternating with 2-cm-thick continuous mudstones. Locally, a restricted trace-fossil assemblage may be present. This facies has good reservoir quality and overlies the bayhead-delta distributary channel facies. Thickness ranges from 5 to 7 m. The gamma-ray log signature shows an irregular, but clearly fining-upward, profile. The sediments are interpreted to be inclined heterolithics tidal point bars, reflecting lateral migration of the bayhead-delta distributary channels. The abundance of inclined shale intervals increases toward the top of the succession. Sandstone intervals containing tidal mud drapes also are more abundant in the top part of this facies. These trends lead to a subdivision into IHS (inclined heterolithic stratification) tidal point-bar base and top facies.

As with the bayhead-delta distributary channel facies, we emphasize modeling the mud drapes and couplets for the geopseudo upscaling exercise. The base facies features cross-bedding throughout and contains a significant proportion of mud drape intervals. Only a few 2-cm-thick shale intervals are encountered. No evidence of bottomset lamination has been found. The angle of inclination ranges from 5 to 19°, which reflects the typical increase in inclination angle upward in the tidal point-bar succession (Thomas et al., 1987). Compared to the base facies, mud drape intervals in the top facies are much thicker and more frequent (Table 2). The shale intervals are equally thick, but they are encountered more often. The inclination angle is constant at 19°, typical of the upper part of the tidal point-bar facies. The overall permeability across the structures is two orders of magnitude (Table 3). The shale intervals are not characterized with the probe-permeameter. In the geopseudo upscaling models, we used values derived from the marine shale facies.

Delta-Front Turbidites: Distal and Proximal Facies

These sediments were cored in wells north of the Countess YY pool in another incised valley

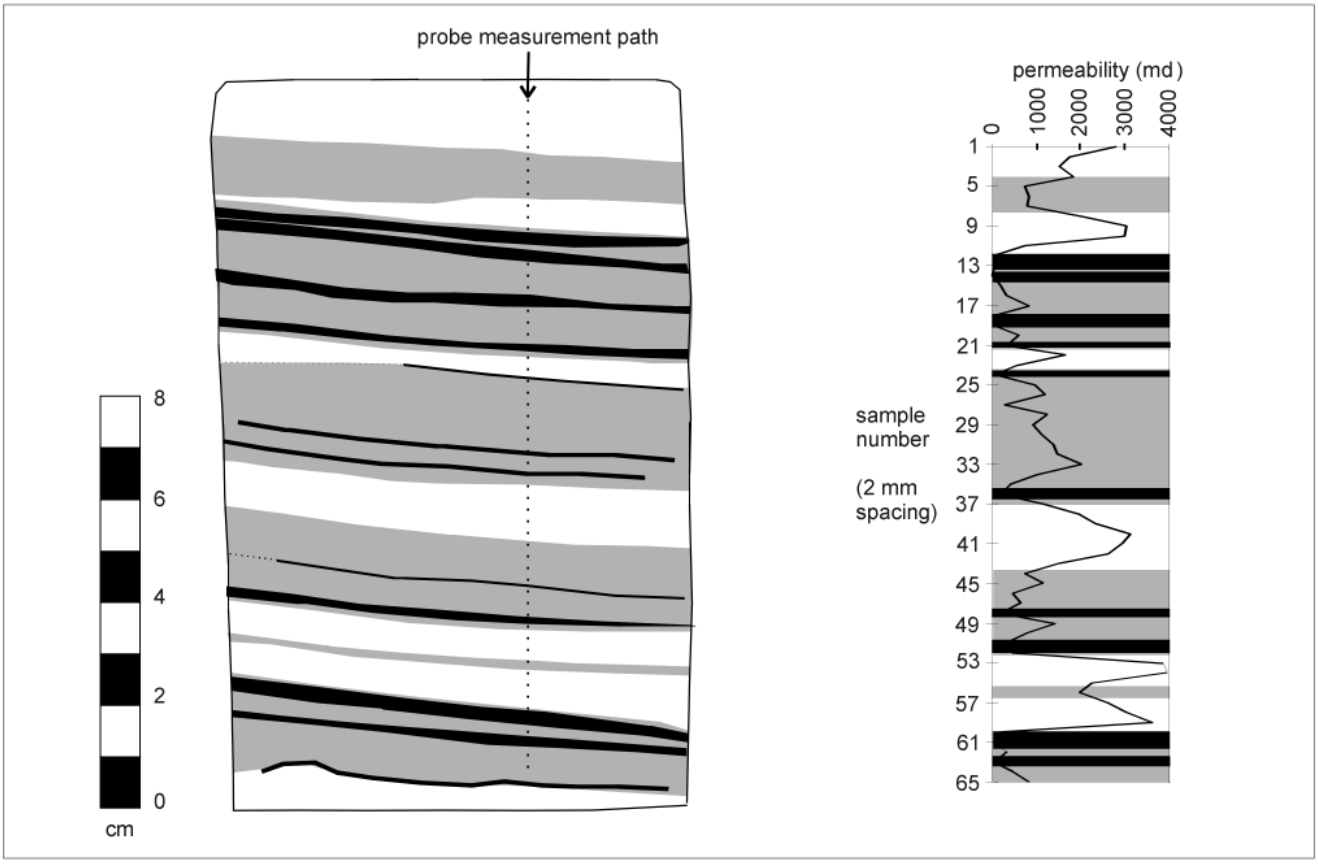

Figure 4—Sketch of a bayhead-delta top facies halved core sample with its corresponding probe-permeameter profile on a linear scale. The sedimentary structures represented in this sample are light laminae (white), dark laminae (shaded), and mud drapes/couplets (black) showing a permeability contrast of two orders of magnitude.

reservoir, and were not described in the paper by Broger et al. (1997). These facies consist of a regular interbedding of planar to wavy parallel-laminated sandstones and weakly burrowed, dark-gray mudstones. Locally, an abundance of wave-generated physical sedimentary structures are present, such as flow ripple lamination. Fine mud laminae are present in some intervals. The mudstone beds are locally highly carbonaceous, and typically much thinner than the intervening sandstone beds (1–5 cm thick). They commonly contain convolute laminations, syneresis cracks, and small-scale gravity faults. Bioturbation is rare in the sandier portions of the facies, but increases in the mudstone interbeds. The trace-fossil assemblage is restricted in diversity (*Planolites, Teichichnus, Cylindrichnus, Skolithos,* and *Tigilllites*), indicating salinity fluctuations or water turbidity. The heterolithic character indicates repeated fluctuations in the energy regime, and the sedimentary structures reflect wave and storm processes. The deformation features indicate failure of the heterolithic succession with depositional relief.

The deposits are encountered in a position lateral to the bayhead-delta distributary channel and IHS tidal point-bar facies, with thicknesses ranging from 8 to 24 m. The gamma-ray log clearly shows an irregular alternation of clean sandstone and shale intervals. Reservoir properties were estimated from well-log data because no core-plug data were available for this study. Reservoir properties and thicknesses of the sandstone intervals increase upward, suggesting a sanding and coarsening-upward trend that indicates progradation. This facies is interpreted to be deposited in a bayhead delta-front turbidite environment, and is inferred to have a lobelike geometry. In some wells, the successions show overall lower porosity and permeability values than elsewhere, indicating an areal variation in grain size or sand proportion. This observation leads to a subdivision into delta-front turbidite distal (lower properties) and proximal (higher properties) facies.

Because core of this facies was not available for observation at the time this study was done, no measurements of the sedimentary structures were

made, and no probe-permeameter measurements were acquired; therefore, this facies is not included in the geopseudo upscaling exercise.

Central Basin Facies

These sediments consist of fine-grained, rippled, flaser-bedded and tidally bedded sandstones displaying abundant shale laminae and double mud drapes with a low-diversity ichnofossil assemblage. This facies has poor reservoir quality and occurs in intervals with a thickness of 1 up to about 5 m at various stratigraphic positions, most commonly on top of estuarine sandstone facies and below marine shales or the Middle Glauconite channel sediments. The gamma-ray log signature is irregular and of intermediate values. This facies is interpreted to have been deposited in the central basin environment, an estuarine body of water representing the prodelta region of the bayhead delta. This facies is not modeled for the geopseudo upscaling exercise due to the abundance of sedimentary structures and burrows, which makes its appearance very complex.

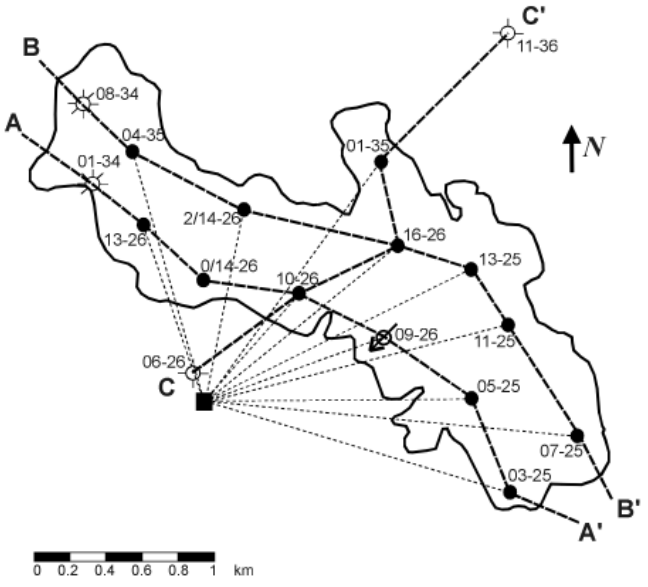

Figure 5—Countess YY pool cross section base map. Dotted lines indicate well trajectories from the single surface drilling pad. Cross sections AA′, BB′, and CC′ are shown in Figure 6.

Marine Shales Facies

These sediments are not encountered in core, but on logs these units of up to 5 m thickness show a high and irregular gamma-ray response, indicating a high shale content. This poor-reservoir-quality facies is interpreted to be deposited as marine shales. They form the uppermost facies within the Lower Glauconite channel, and act as a seal where present. This facies is not a candidate for the geopseudo upscaling exercise due to the lack of sedimentary structures.

Middle Glauconite channel

The Middle Glauconite channel sediments consist of fine-grained, massive to low-angle laminated, flaser to tidally bedded sandstones displaying rare mud drapes. On logs, the succession fines upward into mudstones. The presence of a low-diversity ichnofossil assemblage, tidal bedding features, and occurrence within an incised valley system leads to a tidally influenced estuarine interpretation. This poor-reservoir facies overlies or incises into the Lower Glauconite channel in all wells, and forms a seal to the hydrocarbon-bearing interval below.

LOWER GLAUCONITE CHANNEL EVOLUTION

The internal facies architecture of the Lower Glauconite channel has been correlated for three cross sections that are both parallel and perpendicular to the inferred paleocurrent direction using the vertical facies distribution in the wells (Figures 5, 6). We attempt to relate the reservoir architecture to the incised valley facies model previously described. The areal extent of the various facies is mapped in time to unravel the depositional history of the Lower Glauconite channel. The successive evolutionary stages are illustrated in Figure 7.

After incision of the system and initial deposition by a northward-flowing and prograding braided fluvial system (phase 1), deposition of central basin fines occurs (phase 2). The retreat of the fluvial facies marks the onset of transgression. A bayhead-delta distributary channel system progrades northward in three successive stages (phases 3–5), and is accompanied by IHS tidal point-bar and delta-front turbidite sediments. The ongoing transgression causes the bayhead-delta system to step back, and again deposition of central basin fines occurs across the area (phase 6). The final phase of the transgression is marked by deposition of marine shales, which are also deposited during the high-stand phase (phase 7/8). Finally, the Middle Glauconite channel is initiated during a subsequent fall in relative sea level.

When comparing this reconstruction to the incised valley facies model, many similarities can be found, which justifies the use of this conceptual model as a guide in creating the 2-D simulation models described in following sections. Not only do the facies types correspond to those in the

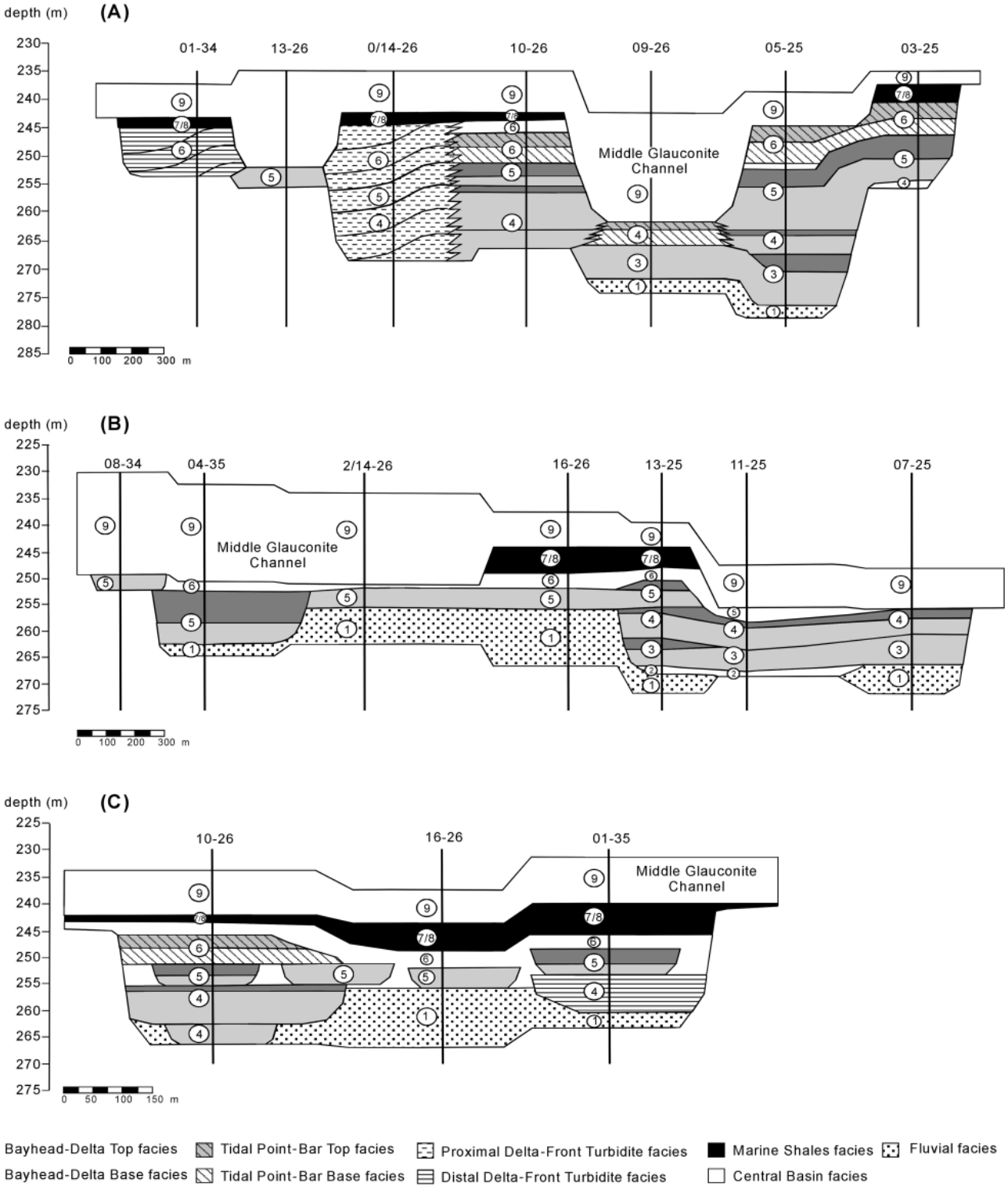

Figure 6—Structural cross sections (see Figure 5 for locations) across the Countess YY pool, showing the correlation of the vertical facies distribution in each well. The circled numbers represent evolutionary stages as shown in Figure 7. (A) Cross section AA′ parallel to the incised valley trend along the southern margin of the Countess YY pool. (B) Cross section BB′ parallel to the incised valley trend along the northern margin of the Countess YY pool. (C) Cross section CC′ perpendicular to the incised valley trend across the center of the Countess YY pool. This section also represents simulation models C1 and C2.

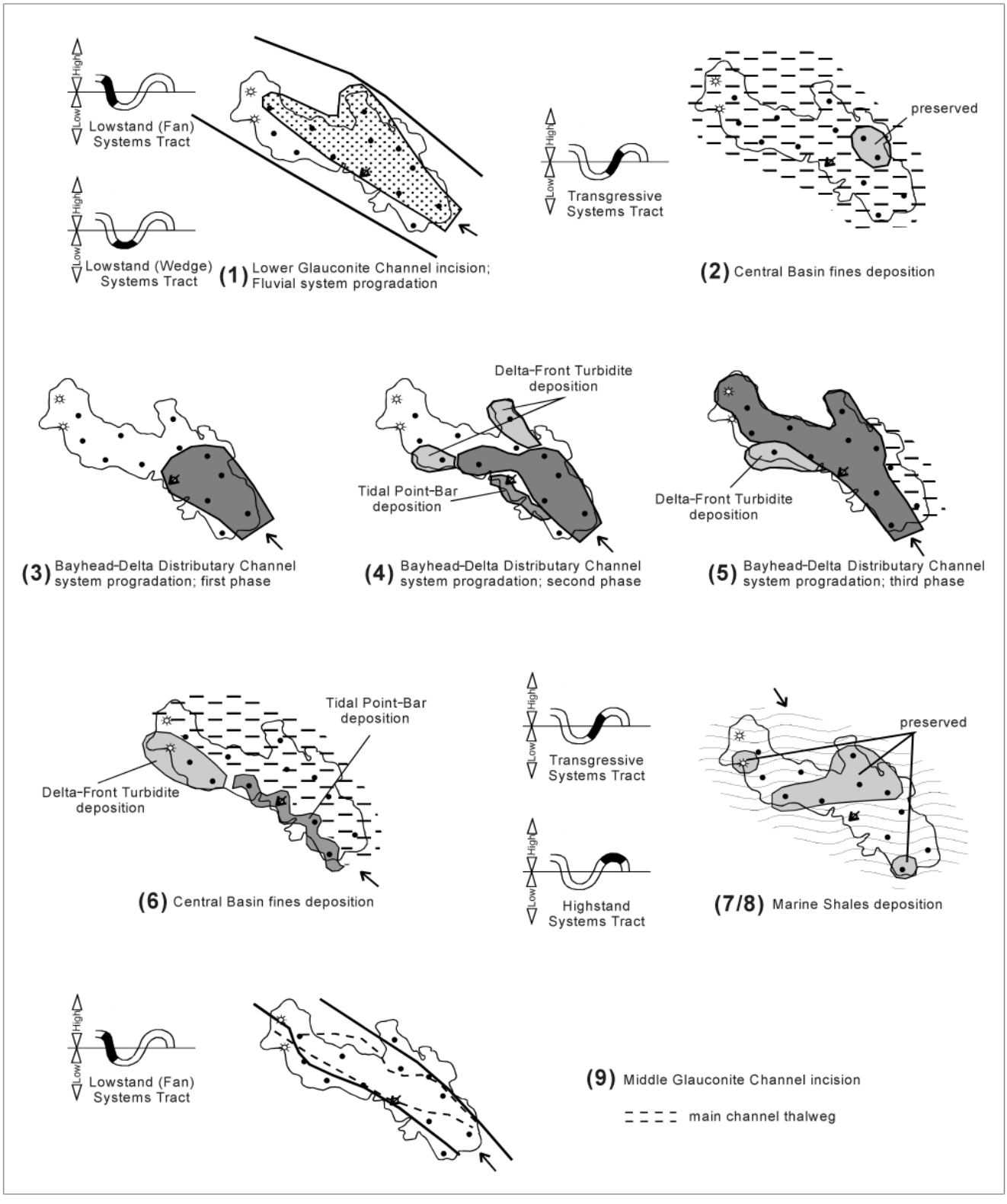

Figure 7—Depositional history of the Lower Glauconite channel showing evolutionary stages over a complete relative sea level cycle, followed by incision of the younger Middle Glauconite channel. Arrows indicate inferred paleocurrent directions.

model for the outer segment 1, but the evolution of the system in response to relative sea level fluctuations is also in agreement with the model; however, we could not identify any barrier island, flood tidal delta, tidal inlet, or washover sediments that should be present in segment 1 of a wave-dominated incised valley system. We believe that these facies were once deposited, but subsequently eroded by deposition of the marine shales or by incision of the Middle Glauconite channel.

GEOPSEUDO UPSCALING EXERCISE

Method

Geological models commonly are upscaled or averaged for use in a reservoir simulator. Geopseudo upscaling is a method that attempts to incorporate successive scales of geological heterogeneity into effective fluid-flow functions. The scales of heterogeneity used are based on the inherent geological hierarchy in sedimentary and sequence stratigraphic systems. On the field scale, fluid flow is dominated by viscous forces, and capillary forces are negligible; however, on a small scale, capillary and viscous forces interact with sedimentary structures, such as laminae. Viscous forces drive oil out of and along high-permeability laminae, and capillary forces drive oil from low-permeability laminae into high-permeability laminae by imbibition. The orientation of the laminae plays a key role in the two-phase displacement process. For example, flow along horizontally arranged laminae will show improved sweep efficiency, whereas flow across vertically arranged laminae will be hindered, resulting in capillary trapping of oil (Ringrose et al., 1993). This interaction of viscous and capillary forces with small-scale sedimentary structures must be captured within effective two-phase flow functions, or pseudo functions. Flow within each simulation model grid block is represented by saturation-dependent functions for the mobility of each phase, known as relative permeability functions. Pseudo relative permeability functions are essentially the calculated effective multiphase flow properties for a given medium under given flow conditions. In the geopseudo upscaling procedure, these pseudo functions are generated for each heterogeneity scale for both the vertical and horizontal flow directions, and then incorporated into models at a larger scale. The effects of sedimentary structures thus are systematically incorporated into the pseudo flow functions for the grid blocks in the full-field model. This method also corrects for numerical dispersion effects caused by the use of large grid blocks in a simulation model. For a more detailed explanation of this technique, refer to Corbett et al. (1992), Ringrose et al. (1993), and Pickup et al. (1994).

Procedure

The core observations and probe-permeameter data are integrated into generalized geopseudo upscaling models for each facies. Cross-bedding and mud drapes are modeled on a millimeter scale, whereas the alternation of massive, cross-bedded and mud-draped intervals is modeled on a decimeter scale. These two upscaling steps result in meter-scale facies-specific grid blocks that are used to populate the 2-D cross sectional simulation models. These models do not exactly match geological reality; they merely try to capture the degree of heterogeneity present. Examples of geopseudo upscaling models are given in Figure 8.

For the purpose of this study, simple 2-D water-oil displacement experiments are simulated using the ECLIPSE reservoir simulator with one water injection well and one producing well at the outer edges of the models. Production rates and time steps are calculated for each model such that two pore volumes of water are flooded through them. Waterflood performance that is influenced by small-scale sedimentary structures may be different in the horizontal and vertical directions; therefore, each model is run twice, once to assess horizontal flow performance and once to assess vertical flow performance, by rotating the model 90°, resulting in two sets of pseudo functions. In the vertical flow models the densities of the phases are set to zero to cancel out the effects of gravity.

The millimeter-scale models are run with the original relative permeability rock curves. Ideally, one should use facies-specific curves, but no relative permeability data were available for the Countess YY pool. Instead, one set of curves originating from an unknown facies in the nearby Countess D incised valley reservoir is used. The D curves were scaled down to the correct YY end points derived from wireline logs. The PSEUDO module in ECLIPSE is run to calculate average reservoir properties and pseudo functions according to the Kyte and Berry method (Kyte and Berry, 1975). The saturation endpoints of the pseudo functions are kept constant. Directional pseudo functions and averaged reservoir properties thus obtained for the millimeter-scale models are subsequently used as input for the decimeter-scale models. Results from the decimeter-scale models are then used as input for the facies-specific grid blocks in the 2-D simulation models (Table 4).

Results

Differences in flow performance among the various models occur only as a result of internal structural arrangements, permeability values, and the

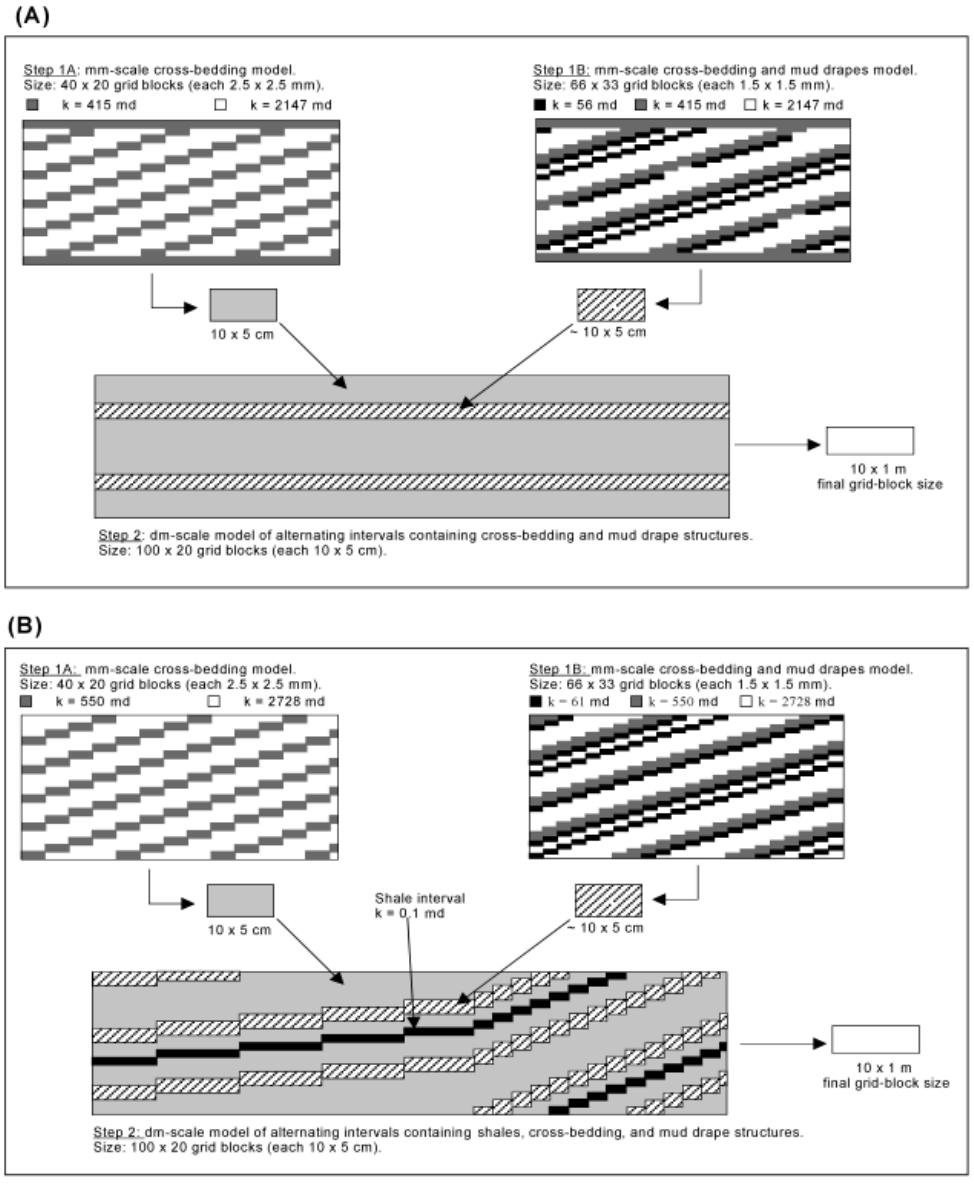

Figure 8—Examples of generalized upscaling models created by integration of core observations and probe-permeameter measurements. To correctly capture the geological heterogeneity in the final grid-block size, two upscaling steps are required. (A) Upscaling model for the bayhead-delta top facies, which features continuous horizontal intervals with cross-bedding structures and intervals with cross-bedding structures accompanied by mud drapes/couplets. (B) Upscaling model for the tidal point-bar base facies, which features inclined intervals with cross-bedding structures, intervals with cross-bedding structures accompanied by mud drapes/couplets, and thin shale intervals. The inclination of these intervals increases upward. Upscaling models of the other facies are built according to the same principle; differences exist in permeability values and in the distribution, thickness, and inclination of the various structures and intervals.

interaction of structures with the fluid displacement process; all models have similar gridding and flow parameters. From the saturation and interblock flow profiles of the millimeter-scale models, we observed that capillary forces expel oil from low-permeability laminae and mud drapes into high-permeability laminae, where it is transported further toward the producing well by viscous forces. In Figure 9, a homogeneous model without sedimentary structures is compared to models with increasing heterogeneity; i.e., increasing permeability contrast across sedimentary structures (note that gravity drainage is rather extreme in the homogeneous model due to a high permeability value of 7730 md). From Figure 9 it is apparent that the waterfront steepens as heterogeneity increases, which effectively delays water breakthrough. This effect is most obvious when the permeability contrast between the structures is one or more orders of magnitude, hence it is less evident in the fluvial cross-bedding model. Based on this observation, we assume that the pseudo curves for the fluvial model account only for numerical dispersion effects, and that they can be used as a comparison to other models to assess the impact of small-scale heterogeneity superimposed upon numerical dispersion effects. At the millimeter scale, the most significant changes in the shape of the pseudo curves are observed in the mud drape models (Figure 10), which can be explained by the presence

Table 4. Averaged Reservoir Properties per Facies Obtained from the Geopseudo Upscaling Exercise*

Facies Type	Porosity (Fraction)	K_h (md)	K_v (md)	K_v/K_h Ratio
Fluvial	0.25	3789	2457	0.65
Bayhead-delta distributary channel base	0.27	1891	1102	0.58
Bayhead-delta distributary channel top	0.27	1330	988	0.74
IHS tidal point-bar base	0.28	1615	1207	0.75
IHS tidal point-bar top	0.25	1238	905	0.73

*K_v = vertical permeability, K_h = horizontal permeability.

of two orders of magnitude permeability contrast. At the decimeter scale, the most significant changes are observed in the tidal point-bar facies, which can be explained by the high degree of heterogeneity caused by the abundance of mud drapes and inclined shale intervals.

From the oil recovery efficiency curves of the decimeter-scale models (Figure 11), we observed that heterogeneity has a negative impact on vertical flow performance compared to horizontal flow performance. The bayhead-delta facies have a recovery efficiency comparable to or even better than the fluvial facies. An explanation for this can be found by looking at the saturation profiles. Water saturation values appear to be highest in the horizontally continuous low-permeability mud drape intervals; oil is expelled from these and brought into the higher permeability cross-bedded intervals, where it is effectively transported to the producer. Thus, heterogeneity can positively contribute to a better sweep efficiency; however, in reality these intervals might not be as laterally continuous as modeled here. From Figure 11, one can see that the recovery efficiency of the tidal point-bar facies is significantly less compared to the other facies. As expected, the presence of inclined shales in these facies prevents good sweep efficiency.

Table 4 shows the pseudo averaged reservoir properties per facies obtained from this exercise. This table shows some significant differences compared to averages based on core-plug values (Table 1). Probe-permeameter data, the basis for the geopseudo upscaled values, are sometimes derived from only one halved core sample for a facies; however, facies-specific core-plug averages are sometimes based on only a few core plugs. A significant amount of uncertainty is involved in both data sets. This uncertainty could be reduced by acquiring probe-permeameter data covering the complete cored sections.

HETEROGENEITY MODELING AND SIMULATION RESULTS

To meet the objectives of this study, we created seven different sensitivity models, in which all facies are present, for cross section CC′ perpendicular to the inferred paleoflow direction. The simulation results are summarized in Table 5. For each model, a 2-D water-oil displacement simulation is performed during a period of 6000 days, with a hypothetical water injection well, injector 1, placed at the center of the model close to the location of well 16-26. Production rates of Countess YY wells are scaled down according to the ratio of 3-D reservoir to 2-D model pore volume to obtain realistic rates for the two hypothetical producing wells, producer 1 to the left near the location of well 10-26, and producer 2 to the right near the location of well 01-35. The injection rate is controlled by a voidage replacement scheme. Because of gravity and the general fining-upward trend within the reservoir, injected water slumps down toward the high-permeability fluvial facies in the aquifer (see Figure 3 for the location of the oil-water contact). Thus, oil displacement occurs mainly by rising of the oil-water contact. To avoid severe coning and high watercuts, perforations are limited to the higher parts of the reservoir. All models have similar gridding and flow parameters; thus differences in flow performance only occur as a result of reservoir architecture, permeability values, and the interaction of facies with the fluid displacement process.

Comparison of Modeling Approaches and Microscale Heterogeneity Impact

As stated in the objectives, we compare three different modeling approaches:

- Layercake model C3 (Figure 12A)
- Reservoir architecture model C2 (Figure 12B)
- Geopseudo upscaled model C1 (Figure 12C)

The C1 and C2 models have poorer sand-body connectivity compared to layercake model C3 because bayhead-delta distributary channels are embedded in poor-reservoir-quality central basin fines, and because the shales in the delta-front turbidite facies are modeled here as low-perme-

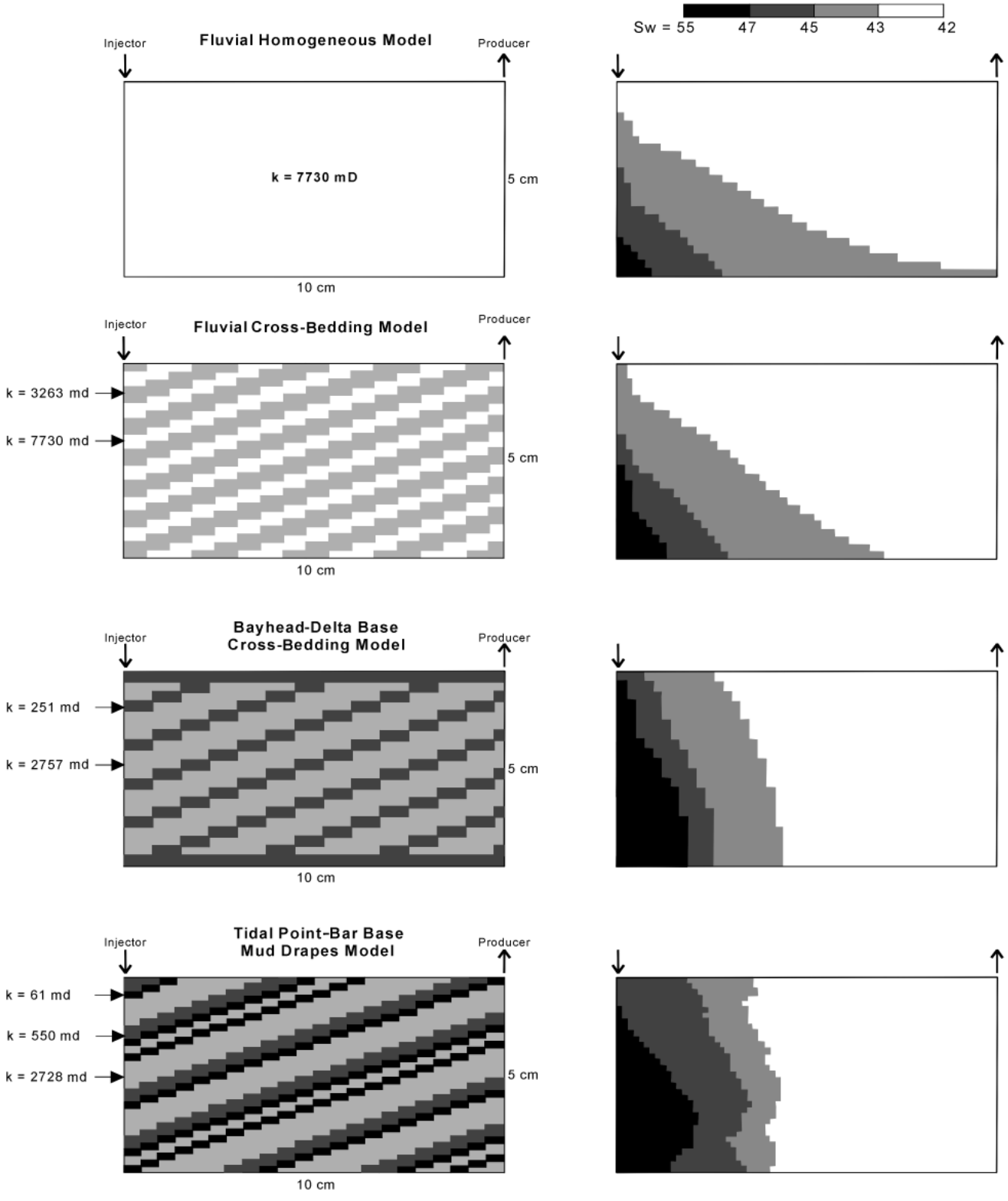

Figure 9—Examples of water saturation profiles after 0.1 days water injection of millimeter-scale upscaling models showing an increased steepening of the waterfront with increasing permeability contrast across the structures. The underlying sedimentary structures and permeability values are shown to the left, and the corresponding water saturation profiles are shown to the right.

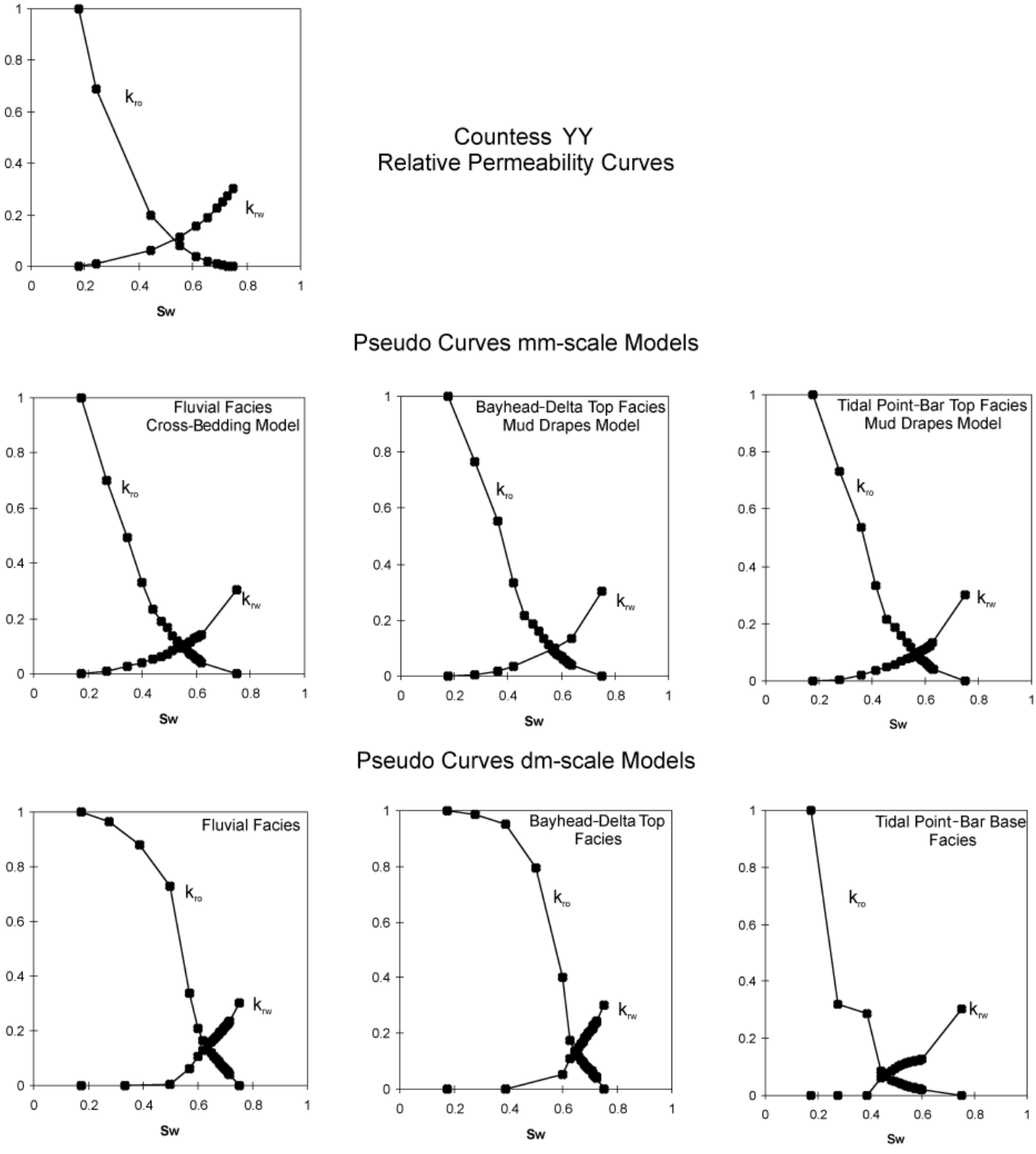

Figure 10—Examples of pseudo relative permeability curves obtained from the geopseudo upscaling exercise. The pseudo curves represent not only the effects of small-scale sedimentary structures on fluid-flow behavior, but also numerical dispersion effects.

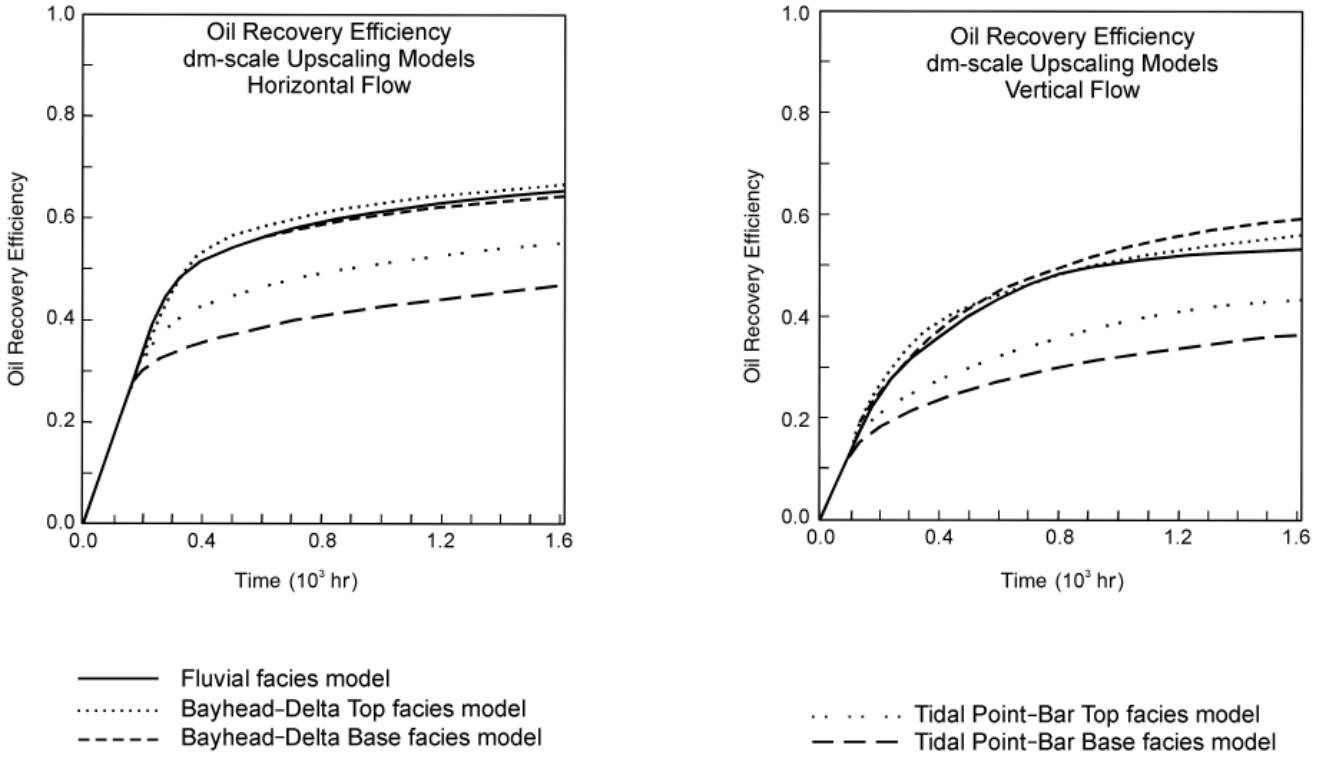

Figure 11—Comparison of oil recovery efficiency curves of the facies-specific decimeter-scale upscaling models for both horizontal and vertical flow performance. Oil recovery efficiency is defined as [(initial oil in place–current oil in place)/initial oil in place].

ability barriers. Model C3 has a stable, gradual rise of the oil-water contact, whereas the waterfront in the other two models is clearly affected by the presence of shales and by poorer sandbody connectivity.

The C1 and C2 models appear to give identical results when fieldwide production data are analyzed; however, differences become apparent when well-specific data are examined (Figure 13; Table 5). Oil recovery of producer 1 in model C1 is 7% less than that of model C2. This difference can be explained by the presence of the tidal point-bar facies in this well's drainage area that were predicted to have poorer performance from the geopseudo upscaling exercise. This difference is confirmed by slightly earlier water breakthrough and a steeper increase in water cut. In producer 2, oil recovery in model C1 is 8% higher than that of model C2, which can be explained by the presence of fluvial and bayhead-delta facies that were predicted to result in better performance. This result is confirmed by later water breakthrough. The expected effects from using the geopseudo upscaling results are thus confirmed. The reverse results seen in both wells cancel out in the fieldwide production data, but it has been shown here that using geopseudo curves and incorporating microscale heterogeneities in fluid-flow simulations does make a significant difference in individual well production performance, depending on the facies types involved.

Fieldwide production data indicate that model C3 has an optimistic performance (11% higher field cumulative oil recovery compared to that of base case model C1), which can be explained by the low degree of heterogeneity and good reservoir connectivity in this model. Modeling the geology as a layercake may cause significant errors in production forecasting.

Mesoscale Heterogeneity Impact

The facies distribution in cross section CC′ is constrained by data from three wells. Significant uncertainty is involved in correlating facies in the interwell area. A large number of possible realizations could be created, but for the purpose of this study only three cases are generated:

- A worst-case model C4 (Figure 14A)
- A best-case model C5 (Figure 14B)
- An intermediate model C1 (Figure 6C)

Table 5. Summary of Two-Dimensional Cross Section Simulation Results

Methodology and Microscale Heterogeneity Models	Unit	C1 Base Case Model	C2 Averaged Model Results	C2 Averaged Model Change from C1	C3 Layercake Model Results	C3 Layercake Model Change from C1
Field cumulative oil recovery @ 6000 days	10^3 m^2	13.5	13.5		15.0	+11%
Producer 1 cumulative oil recovery @ 6000 days	10^3 m^2	7.0	7.5	+7%	8.0	+14%
Producer 2 cumulative oil recovery @ 6000 days	10^3 m^2	6.5	6.0	–8%	7.0	+8%
Field oil recovery efficiency @ 6000 days	Fraction	0.35	0.35		0.4	+14%
Initial oil in place	10^3 m^2	38	38		39	+3%
Field water breakthrough time	Days	300	325	+25	325	+25
Producer 1 water breakthrough time	Days	300	325	+25	325	+25
Producer 2 water breakthrough time	Days	550	480	–70	450	–100

Mesoscale Heterogeneity Models	Unit	C1 Base Case Scenario	C4 Worst-Case Scenario Results	C4 Worst-Case Scenario Change from C1	C5 Best-Case Scenario Results	C5 Best-Case Scenario Change from C1
Field cumulative oil recovery @ 6000 days	10^3 m^2	13.5	11	–19%	15	+11%
Producer 1 cumulative oil recovery @ 6000 days	10^3 m^2	7	6	–14%	8	+14%
Producer 2 cumulative oil recovery @ 6000 days	10^3 m^2	6.5	5	–23%	7	+8%
Field oil recovery efficiency @ 6000 days	Fraction	0.35	0.31	–11%	0.37	+6%
Initial oil in place	10^3 m^2	38	35.5	–7%	40	+5%
Field water breakthrough time	Days	300	280	–20	310	+10
Producer 1 water breakthrough time	Days	300	280	–20	340	+40
Producer 2 water breakthrough time	Days	550	950	+400	560	+10

Macroscale Heterogeneity Models	Unit	C1 Base Case Container	C6 Big Container Results	C6 Big Container Change from C1	C7 Small Container Results	C7 Small Container Change from C1
Field cumulative oil recovery @ 6000 days	10^3 m^2	13.5	14.5	+7%	13	–4%
Producer 1 cumulative oil recovery @ 6000 days	10^3 m^2	7	7.5	+7%	6.75	–4%
Producer 2 cumulative oil recovery @ 6000 days	10^3 m^2	6.5	7	+8%	6	–8%
Field oil recovery efficiency @ 6000 days	Fraction	0.35	0.325	–7%	0.375	+7%
Initial oil in place	10^3 m^2	38	43	+13%	35	–8%
Field water breakthrough time	Days	300	300		340	+40
Producer 1 water breakthrough time	Days	300	300		340	+40
Producer 2 water breakthrough time	Days	550	510	–40	660	+110

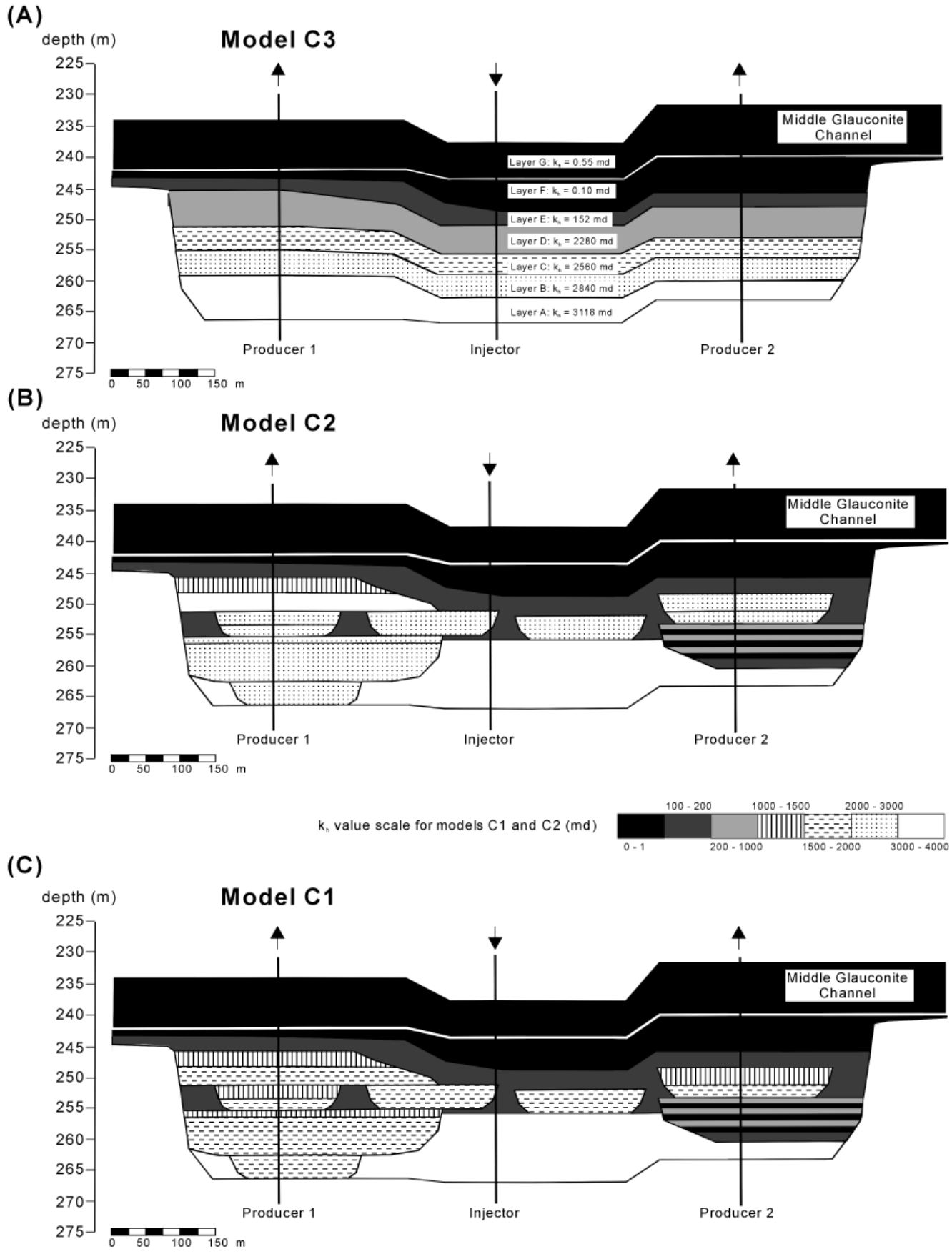
(A)
depth (m)
Model C3
225
230
235
240
245
250
255
260
265
270
275
Middle Glauconite Channel
Layer G: k_h = 0.55 md
Layer F: k_h = 0.10 md
Layer E: k_h = 152 md
Layer D: k_h = 2280 md
Layer C: k_h = 2560 md
Layer B: k_h = 2840 md
Layer A: k_h = 3118 md
Producer 1
Injector
Producer 2
0 50 100 150 m
(B)
depth (m)
Model C2
Middle Glauconite Channel
Producer 1
Injector
Producer 2
0 50 100 150 m
k_h value scale for models C1 and C2 (md)
100 - 200
1000 - 1500
2000 - 3000
0 - 1
200 - 1000
1500 - 2000
3000 - 4000
(C)
depth (m)
Model C1
Middle Glauconite Channel
Producer 1
Injector
Producer 2
0 50 100 150 m

Figure 12—Horizontal permeability distribution in simulation models C1, C2, and C3. (A) Layercake model C3 with averaged permeability values per layer based on core-plug values (Table 6). (B) Reservoir architecture model C2 with averaged permeability values per facies based on core-plug values (Table 1). (C) Geopseudo upscaled model C1 with pseudo-averaged permeability values per facies based on probe-permeameter data (Table 4).

All three models use results from the geopseudo upscaling exercise. By comparing Figures 14 and 6C, it can be seen that the most important factors discriminating between these models are the proportion of good-reservoir-quality facies and the level of sand-body connectivity. The fluvial facies as modeled in C1 and C5 is interpreted to be a sheet of amalgamated braided fluvial sandstone bodies. An alternative correlation shown in model C4 confines the upper portion of this braided system to a narrower, isolated channel. The most important difference among the three models is the variation in dimension of the bayhead-delta distributary channels. From sand-body thickness encountered in core it is possible to predict a range of channel widths using different relationships published by Fielding and Crane (1987). Table 7 gives the calculations performed for a number of different channel depths. We assume that sand-body thickness as seen in core is the same as the channel depth, thus ignoring preservation and compaction factors. Note, however, that these relationships are based on fluvial channel systems, although we are dealing here with a tidally influenced fluvio-deltaic system. At present, no studies on channel width/depth relationships for these systems are available.

Waterflood performance is poorest for model C4. Saturation profiles indicate that poor sand-body connectivity and lower proportions of good-reservoir facies result in poorly swept zones and hampered flood-front movement. Best performance comes from model C5, where excellent sand-body connectivity and high proportions of good-reservoir facies result in a more stable flood-front movement. These results are not surprising; of greater interest is the fact that the differences in performance can be assessed quantitatively. Production data (Figure 15; Table 5) show significant differences in cumulative oil recovery compared to model C1, with up to 30%

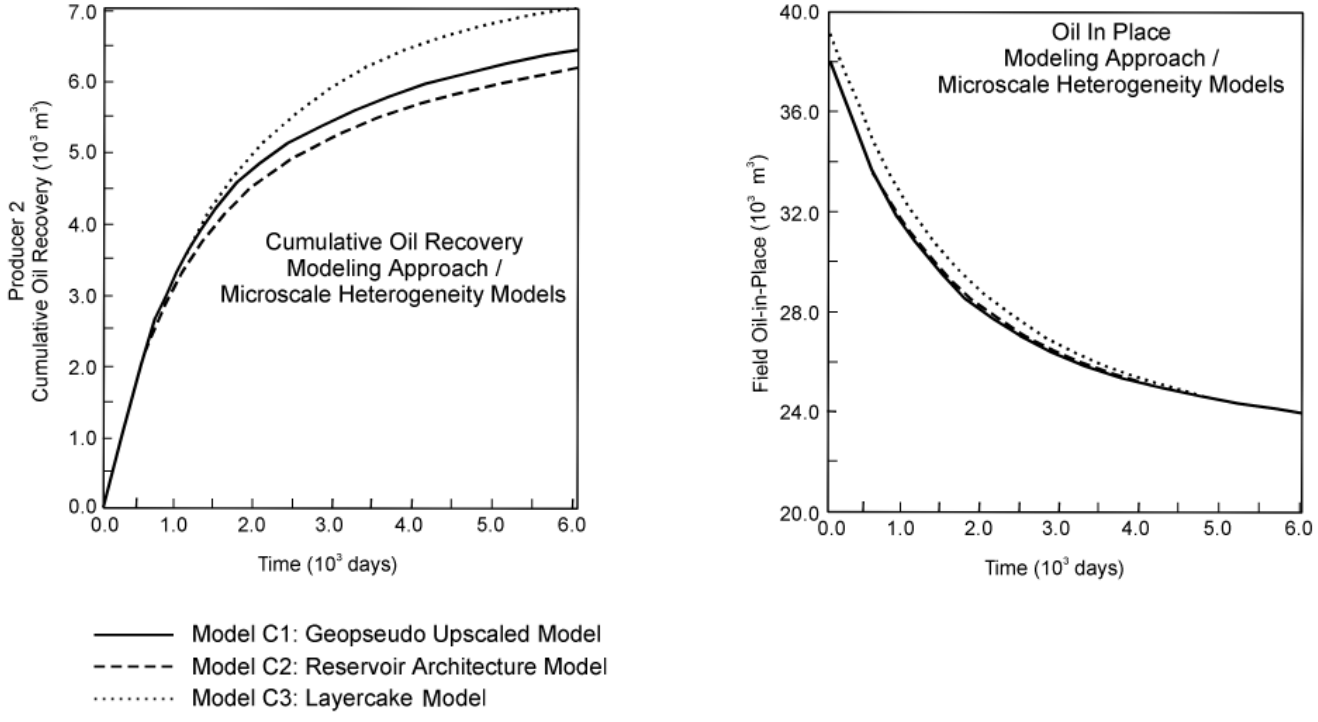

Figure 13—Comparison of simulation results of the three modeling approach/microscale heterogeneity sensitivity models. Note that cumulative oil recovery curves are given for well producer 2 only to show the difference between models C1 and C2 (see text for explanation).

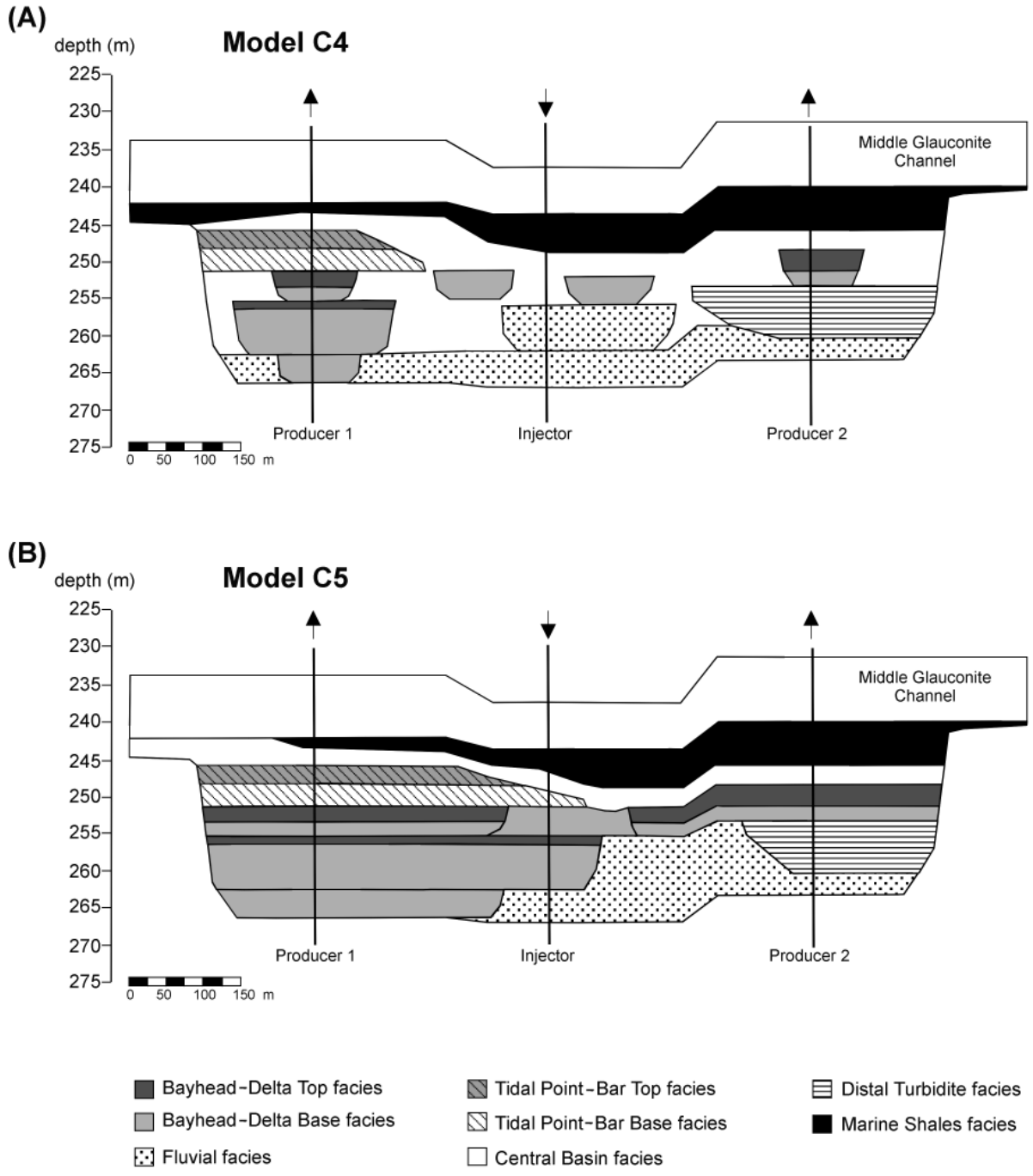

Figure 14—(A) Worst-case facies distribution model C4 and (B) best-case facies distribution model C5 as used in the mesoscale heterogeneity sensitivity analysis. Both models are compared to the intermediate-case facies distribution model C1 represented in Figure 6C.

difference between extreme cases C4 and C5. Also, the difference in initial oil-in-place values is not insignificant, with 12% between extreme cases C4 and C5. Note that the performance of layercake model C3 resembles that of the best-case scenario model C5. This similarity suggests that modeling the incised valley geology as a layercake is an optimistic scenario, and that it is more likely that an incised valley reservoir will perform less well. This, of course, depends on the nature of the valley fill. We have shown that mesoscale heterogeneity and the uncertainty in

Table 6. Arithmetically Averaged Reservoir Properties per Layer Based on Core-Plug or Wireline Data*

Layer	Based on Properties of Facies	Porosity (Fraction)	K_h (md)	K_v (md)	K_v/K_h Ratio	Data Source
Layer G	Middle Glauconite	0.10	0.55	0.015	0.03	Core plugs
Layer F	Marine shales	0.05	0.10	–	–	Wireline logs
Layer E	Central basin	0.21	152	22	0.14	Core plugs
Layer D	IHS tidal point bar	0.26	2280	1530	0.67	Core plugs
Layer C	Fluvial**	0.27	2560	1690	0.66	Core plugs
Layer B		0.27	2840	1875	0.66	Core plugs
Layer A		0.25	3118	932	0.30	Core plugs

*K_v = vertical permeability, K_h = horizontal permeability.
**Interpolated between layers D and A.

Table 7. Bayhead-Delta Distributary Channel Width Calculations

Channel Depth, *b*, and Channel Width, *w*, Relationships (from Fielding and Crane, 1987)

Case 1b: channels that have not been allowed to migrate laterally	$w = 0.95(b)^{2.01}$
Case 2a: geometric mean of all fluvial channel types	$w = 12.1(b)^{1.85}$
Case 2b: truly meandering streams	$w = 64.6(b)^{1.54}$

Calculated Channel Widths (sand-body thickness equals channel depth)

Well	Channel Depth (m)	Case 1b Width (m)	Case 2a Width (m)	Case 2b Width (m)
Well 10-26 upper and lower channel and well 16-26	4	15	157	546
Well 01-35	5	24	238	770
Well 10-26 middle channel	7	47	443	1293

Channel Widths Used in Two-Dimensional Simulation Models
(widths <100 m are considered too narrow for grid-block resolution used)

Well	Channel Depth (m)	Worst-Case Width (m)	Base-Case Width (m)	Best-Case Width (m)
Well 10-26 upper and lower channel and well 16-26	4	100	150	500
Well 01-35	5	100	250	700
Well 10-26 middle channel	7	200	400	1200

the facies distribution can introduce major errors in both forecasting production and estimating reserves.

Macroscale Heterogeneity Impact

The extent of the Lower Glauconite channel is defined by integrating well and seismic data, although some degree of uncertainty is involved in interpreting the 3-D seismic data. The good-quality seismic data can pick up only good-porosity zones that are thicker than 4–5 m. One of the pitfalls in interpreting the data is the similarity of the amplitude signature of the Lower Glauconite channel and the stratigraphically lower Ostracod member because their velocities and densities are similar. The truncation of the Ostracod member is one of the criteria for recognizing the incised valley system, but it is difficult to distinguish the two stratigraphic members seismically; moreover, where the Lower Glauconite channel does not incise deep enough to erode the Ostracod, the reflections interfere with each other. From the seismic section corresponding to section CC′, we found that the transition from the amplitude signature of the Lower Glauconite channel into that of the Ostracod member occurs over an interval approximately 50–100 m wide, allowing the generation of three cases:

- A big container model C6 (Figure 16A)
- A small container model C7 (Figure 16B)
- An intermediate model C1 (Figure 6C)

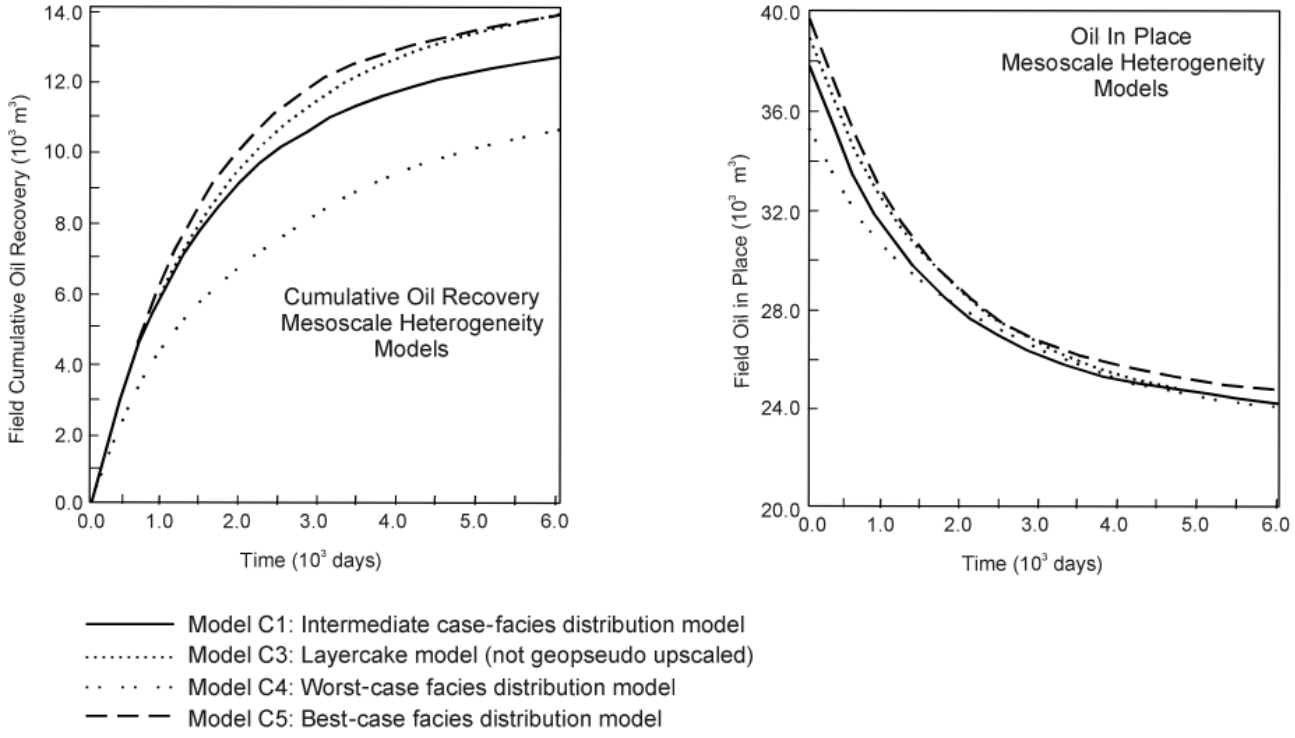

Figure 15—Comparison of total field simulation results of the three mesoscale heterogeneity sensitivity models. The results of layercake model C3 have been added to show the similarity in performance between this model and the best-case facies distribution model C5.

Production data (Figure 17; Table 5) show significant changes in performance, most notably the initial oil-in-place values, where a difference of 21% between extremes is observed. Most oil is recovered from the model with the largest initial oil-in-place value, model C6, but the oil recovery curves for all three models are similar during the bulk of the production period. We have shown that macroscale heterogeneity and uncertainty in seismic interpretation may produce substantial errors in reserves estimation and, to a lesser extent, in production forecasting. Again, this is not surprising, but the oil recovery and oil-in-place numbers obtained in this study do allow a quantitative comparison between all the sensitivity models.

CONCLUSIONS

(1) The facies types recognized in the Lower Glauconite channel and the reconstructed evolution of this system in response to relative sea level changes are in good agreement with the incised valley facies model as proposed by Dalrymple et al. (1992) and Zaitlin et al. (1994). Not identified barrier-island-related facies are assumed to have been eroded by later marine shale and Middle Glauconite channel deposition.

(2) Results from the 2-D geopseudo upscaling exercise predict that small-scale heterogeneity in the highly permeable fluvial facies has no impact on sweep efficiency; however, in the bayhead-delta facies, a permeability contrast of two orders of magnitude is expected to contribute to an improved sweep efficiency. In contrast, inclined shale intervals in the tidal point-bar facies are thought to prevent good sweep efficiency. These predicted effects from the geopseudo upscaling exercise have been confirmed by the results of simulating the 2-D cross-sectional models.

(3) Modeling an incised valley reservoir as a layercake has proved to result in optimistic performance, leading to 11% higher oil recovery when compared to a 2-D geopseudo upscaled model. In a highly favorable scenario, an incised valley reservoir indeed may behave like a layercake, but it is more likely that it will perform less well because of the complex reservoir architecture and high degree of reservoir heterogeneity that may be present.

(4) Applying the geopseudo upscaling method and incorporating microscale heterogeneities or small-scale sedimentary structures in 2-D fluid-flow simulations has proved to make a significant difference in individual well oil recovery (up to 8%), depending on the facies types involved in a well's drainage area.

(5) Incorporating mesoscale heterogeneities modeled as variations in sand-body dimensions and

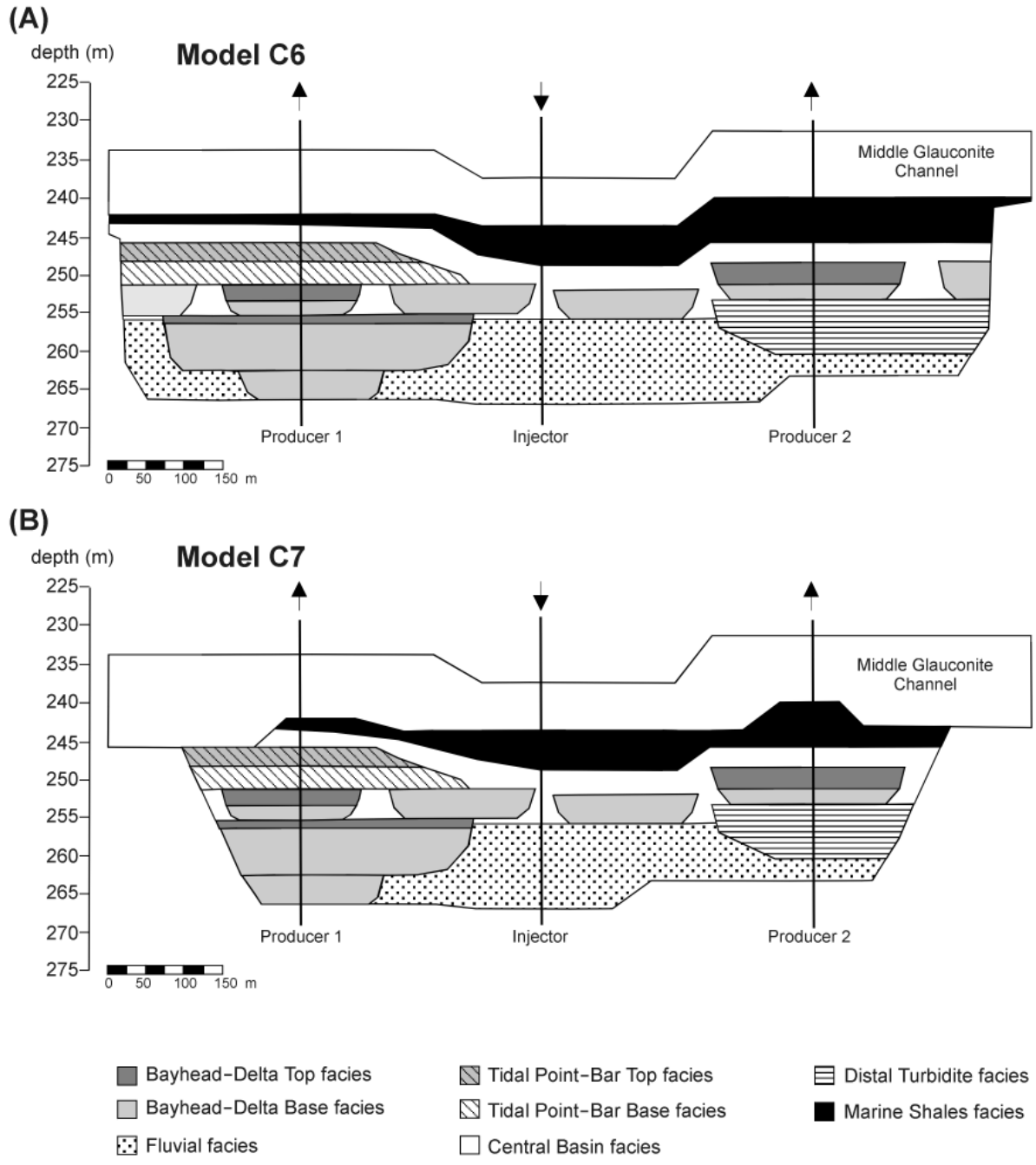

Figure 16—(A) Big container model C6 and (B) small container model C7 as used in the macroscale heterogeneity sensitivity analysis. Both models are compared to the intermediate-case facies distribution model C1 represented in Figure 6C.

connectivities in 2-D fluid-flow simulations has proven to have a major impact on field oil recovery, leading to differences of up to 30% between extremely positive and negative 2-D cases. The impact on original oil-in-place values is not insignificant, with a difference of 12% between extreme 2-D cases.

(6) Incorporating macroscale heterogeneity expressed as variations in incised valley size defined by seismic interpretation in 2-D fluid-flow simulations has proved to have greatest impact on original oil-in-place values, leading to differences up to 21% between extreme 2-D cases. The impact on oil recovery values is not insignificant, with a difference of 11% between extreme 2-D cases.

(7) Not taking into account small-scale sedimentary structures, uncertainty in reservoir architecture,

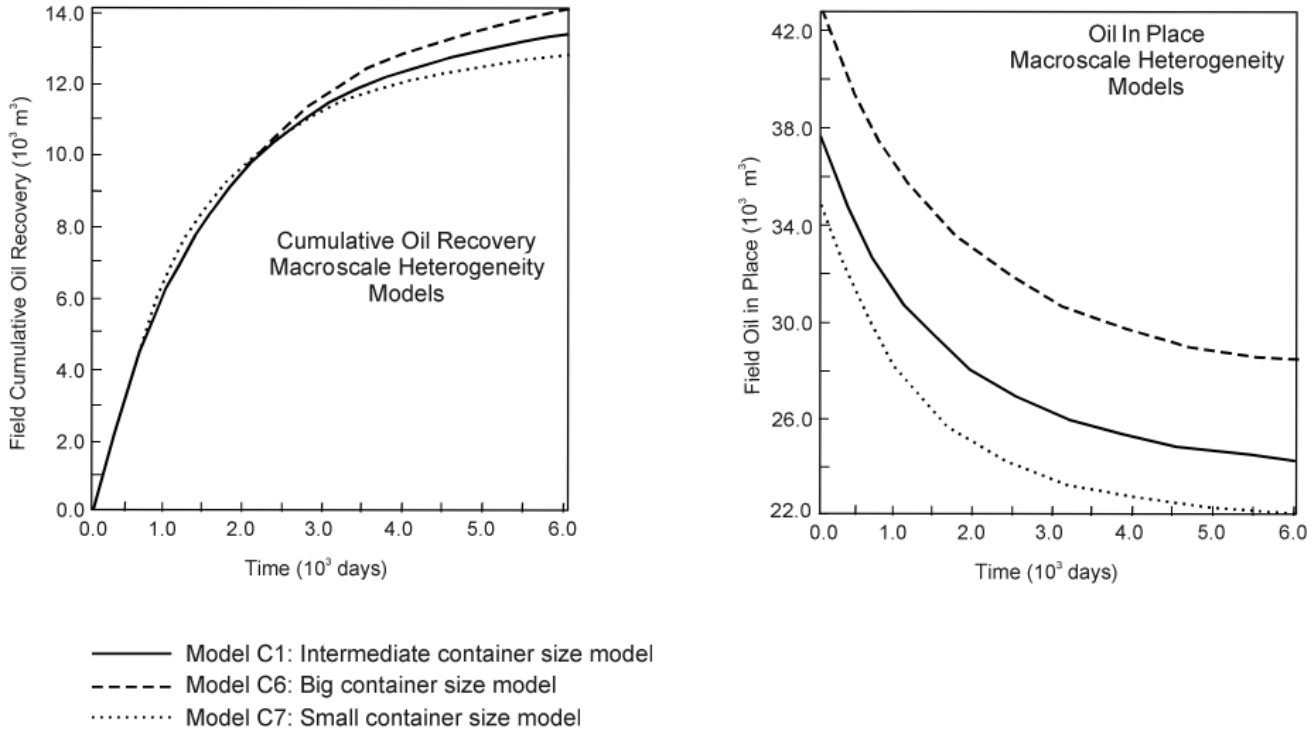

Figure 17—Comparison of total-field simulation results of the three macroscale heterogeneity sensitivity models.

and incised valley size in reservoir simulation studies can introduce substantial errors in reserves estimation and production forecasting

DISCUSSION

The conclusions from this study are only valid for 2-D hypothetical cases and should not be applied directly to practical field situations; moreover, the results are case specific because incised valley-fill geology is highly complex and variable. To fully appreciate the impact and value of the geopseudo upscaling approach, a 3-D geopseudo upscaling exercise should be undertaken. In their paper, Ringrose et al. (1993) stated that certain bedforms, such as a trough cross-bed model, require a detailed 3-D grid model. They showed that the sweep efficiency of a 3-D bedform model may differ considerably from that of a 2-D model. In addition, a full-field 3-D simulation study should be done, which enables direct comparison of simulation results with real production data. When changing parameters in history-matching exercises, one should consider the various uncertainties involved in modeling the complex geology of an incised valley reservoir.

When applying the geopseudo upscaling approach, it is recommended to start a fit-for-purpose data acquisition program early in the life of a field. Ideally, the data set should include core data, probe-permeameter profiles, facies-specific relative permeability curves, well-log data, and seismic data. Outcrop analog or modern depositional environment studies can be used to create more realistic 3-D upscaling models, such that flow perpendicular to and parallel to paleoflow directions can be simulated. Adopting the geopseudo upscaling method does require an increased effort in reservoir description compared to using the simplified layercake or conventional upscaling or averaging methods, but the benefits include more realistic reserves estimation and reservoir performance prediction, enhanced reservoir understanding, and improved reservoir management.

REFERENCES CITED

Broger, E. J. K., G. E. Syhlonyk, and B. A. Zaitlin, 1997, Glauconite sandstone exploration: a case study from the Lake Newell project, southern Alberta, *in* S. G. Pemberton and D. P. James, Petroleum geology of the Cretaceous Mannville Group, western Canada: Canadian Society of Petroleum Geologists Memoir 18, p. 140–168.

Corbett, P. W. M., P. S. Ringrose, J. L. Jensen, and K. S. Sorbie, 1992, Laminated clastic reservoirs: the interplay of capillary pressure and sedimentary architecture: Society of Petroleum Engineers Annual Technical Conference, Paper SPE 24699, presented at the 67th Annual Technical Conference and Exhibition, Washington, 4–7 October, 1992, p. 365–376.

Dalrymple, R. W., B. A. Zaitlin, and R. Boyd, 1992, Estuarine facies models: conceptual basis and stratigraphic implications:

Journal of Sedimentary Petrology, v. 62, p. 1130–1146.
Dolson, J. C., J. Piombino, M. Franklin, and R. Harwood, 1993, Devonian oil in Mississippian and Mesozoic reservoirs—unconformity controls on migration and accumulation, Sweetgrass arch, Montana: The Mountain Geologist, v. 30, p. 125–146.
Fielding, C. R., and R. C. Crane, 1987, An application of statistical modeling to the prediction of hydrocarbon recovery factors in fluvial reservoir sequences, *in* F. G. Ethridge, R. M. Flores, and M. D. Harvey, eds., Recent developments in fluvial sedimentology: SEPM Special Publication 39, p. 321–327.
Halbouty, M. T., ed., 1982, The deliberate search for the subtle trap: AAPG Memoir 32, 351 p.
Kyte, J. R., and D. W. Berry, 1975, New pseudo functions to control numerical dispersion: Society of Petroleum Engineers Journal, August 1975, p. 269–275.
Pickup, G. E., P. S. Ringrose, M. M. Forrester, J. L. Jensen, and K. S. Sorbie, 1994, The geopseudo atlas: geologically based upscaling of multiphase flow: Society of Petroleum Engineers European Petroleum Computer Conference Paper SPE 27565, given at the SPE European Petroleum Conference, Aberdeen, 15–17 March, 1994, p. 277–289.
Pulham, A. J., 1994, The Cusiana field, Llanos basin, eastern Colombia: high resolution sequence stratigraphy applied to late Paleocene–early Oligocene, estuarine, coastal plain and alluvial clastic reservoirs, *in* S. Johnson, ed., High resolution sequence stratigraphy: innovations and applications (abstracts): University of Liverpool, Liverpool, England, p. 63–68.
Ringrose, P. S., K. S. Sorbie, P. W. M. Corbett, and J. L. Jensen, 1993, Immiscible flow behaviour in laminated and cross-bedded sandstones: Journal of Petroleum Science and Engineering, v. 9, p. 103–124.
Thomas, R. G., D. G., Smith, J. M. Wood, J. Visser, E. A. Calverley-Range, and E. H. Koster, 1987, Inclined heterolithic stratification—terminology, description, interpretation and significance: Sedimentary Geology, v. 53, p. 123–179.
Zaitlin, B. A., R. W. Dalrymple and R. Boyd, 1994, The stratigraphic organization of incised valley systems associated with relative sea-level change, *in* R. W. Dalrymple, R. Boyd, and B. A. Zaitlin, eds., Incised-valley systems: origin and sedimentary sequences: SEPM Special Publication 51, p. 45–60.

ABOUT THE AUTHORS

Madeleine Peijs-van Hilten

Madeleine Peijs-van Hilten started her career in 1986 as a reservoir engineering technical assistant with Royal Dutch/Shell in The Hague, Netherlands. In 1989 she entered a geology program at the Department of Earth Sciences of Utrecht University. After receiving her master's degree in 1995, she moved on to Heriot-Watt University in Edinburgh, Scotland, to participate in a M.Sc. course in reservoir evaluation and management. Madeleine received the SPE-funded Colin Robertson Memorial Prize for her capabilities in integrating geoscience and reservoir engineering skills, and graduated with distinction in 1996. Since April 1997 she has been with the reservoir description group of Halliburton Energy Services, where she is involved in integrated reservoir characterization studies.

Timothy R. Good

Tim Good obtained a B.Sc. degree in geology and physical geography from the University of Hull. He later followed the M.Sc. course in sedimentology and its applications at the University of Reading. He graduated from Reading with a Ph.D. after research on the interaction of cold-climate fluvial and eolian sedimentary systems in the United Kingdom (UK) and the Canadian Arctic. Tim joined BP exploration in 1983 and worked as a sedimentologist in Alaska, China, and the UK. In 1992 he joined Heriot-Watt University, Edinburgh, where his research interests were in quantitative sedimentology and reservoir modeling. He has recently joined the reservoir characterization group of Mobil Technology Company.

Brian A. Zaitlin

Brian Zaitlin received his B.Sc. degree from Concordia (Loyola) University in 1979, a M.Sc. degree from the University of Ottawa in 1981, and then worked with Gulf Canada Resources between 1981 and 1983. Brian returned to university to pursue a Ph.D. at Queen's University (Kingston) through early 1987, after which he traveled to the University of Sydney, Australia, on a NSERC postdoctoral fellowship. Brian co-edited CSPG Memoir 16 and SEPM Special Publication 51, was an associate editor of the *CSPG Bulletin*, and a co-recipient of both the CSPG-CWLS Best Oral Presentation Award (1995) and the AAPG-SEPM Excellence in Oral Presentation (1997), and was a 1996–1997 AAPG Distinguished Lecturer. Brian has worked both in technical services groups and as part of front-line exploration teams with Gulf Canada Resources, Imperial Oil (Esso), and is currently with PanCanadian Petroleum Limited as senior technical specialist in clastic sedimentology/sequence stratigraphy. His current research interests include incised valley and marginal marine reservoirs in relation to the exploration for, and exploitation of, hydrocarbons.